Fine-tuning the properties of the thrombin binding aptamer through cyclization: Effect of the 5'-3' connecting linker on the aptamer stability and anticoagulant activity

Claudia Riccardi, Albert Meyer, Jean-Jacques Vasseur, Irene Russo Krauss, Luigi Paduano, François Morvan, Daniela Montesarchio

https://doi.org/10.1016/j.bioorg.2019.103379

Fine-tuning the properties of the Thrombin Binding Aptamer through cyclization: effect of the 5′-3′ connecting linker on the aptamer stability and anticoagulant activity

Claudia Riccardi,[a] Albert Meyer,[b] Jean-Jacques Vasseur,[b]
Irene Russo Krauss,[a,c] Luigi Paduano,[a,c] François Morvan,[b,*] Daniela Montesarchio[a,*]

[a]*Department of Chemical Sciences, University of Naples Federico II, Via Cintia 21, I-80126, Napoli, Italy*

[b]*Institut des Biomolécules Max Mousseron, Université de Montpellier, CNRS, ENSCM, Montpellier, France*

[c]*CSGI – Consorzio Interuniversitario per lo Sviluppo dei Sistemi a Grande Interfase, Via della Lastruccia 3, I-50019, Sesto Fiorentino (Fi), Italy*

*Corresponding authors. E-mail address: daniela.montesarchio@unina.it (D. Montesarchio); francois.morvan@umontpellier.fr (F. Morvan).

ABSTRACT

A small library of cyclic TBA analogues (named cycTBA **I-IV**), obtained by covalently connecting its 5′- and 3′-ends with flexible linkers, has been synthesized with the aim of improving its chemical and enzymatic stability, as well as its anticoagulant properties. Two chemical procedures have been exploited to achieve the desired cyclization, based on the oxime ligation method (providing cycTBA **I** and **II**) or on Cu(I)-assisted azide-alkyne cycloaddition (CuAAC) protocols (for cycTBA **III** and **IV**), leading to analogues containing circularizing linkers with different chemical nature and length, overall spanning from 22 to 48 atoms. The resulting cyclic TBAs have been characterized using a variety of biophysical methods (UV, CD, gel electrophoresis, SE-HPLC analyses) and then tested for their serum resistance and anticoagulant activity under *in vitro* experiments. A fine-tuning of the length and flexibility of the linker allowed identifying a cyclic analogue, cycTBA **II**, with improved anticoagulant activity, associated with a dramatically stabilized G-quadruplex structure (ΔT_m = +17 °C) and a 6.6-fold higher enzymatic resistance in serum compared to unmodified TBA.

KEYWORDS: thrombin binding aptamer, G-quadruplex, biophysical characterization, thrombin, anticoagulant activity

https://doi.org/10.1016/j.bioorg.2019.103379

1. INTRODUCTION

Among the biologically active aptamers, the Thrombin Binding Aptamer (TBA, $^{5'}$GGTTGGTGTGGTTGG$^{3'}$) - adopting a stable chair-like, antiparallel G-quadruplex (G4) structure and able to strongly inhibit fibrin clot formation by its binding to thrombin - has attracted huge attention as effective thrombin activity modulator, representing one of the most extensively studied systems in the development of thrombin-targeting agents.[1–4]

Albeit clinical trials to validate its anticoagulant efficacy have been halted after Phase I studies for its suboptimal dosing profiles,[5] TBA is still actively investigated for its potential applications in therapeutics[4] and diagnostics,[6] mainly in cardiovascular diseases, and a large number of its variants have been described in the literature. In the past decades, both serendipity and targeted rational design have contributed to discover chemically modified TBA analogues endowed with markedly improved physico-chemical and biological properties. Among the approaches thus far explored to obtain modified TBA variants with promising pharmacokinetic profiles, either backbone modifications[7–19] or incorporation onto suitable nanoplatforms - including magnetic,[20–22] gold,[23–27] silica-based nanoparticles[28–31] and graphene[32,33] - have been successfully exploited.

As a general strategy to improve the overall properties of anticoagulant aptamers and obtain TBA analogues better performing *in vitro* and *in vivo*, we have recently explored the cyclization, extending an approach similar to that already adopted for peptides[34] and peptidomimetics,[35] as well as peptide nucleic acids (PNA)[36] and glycomimetics[37,38], but only limitedly investigated for oligonucleotides.[39,40] In this frame, valuable multivalent circular analogues of antithrombotic oligonucleotides have been also studied.[41]

As a proof-of-concept, we have previously synthesized a cyclic TBA analogue obtained by covalently connecting the 3′- and 5′-ends of this G-rich oligonucleotide with a 20 atom long linker, ensuring approximately the same length of a trinucleotide (Figure 1).[42]

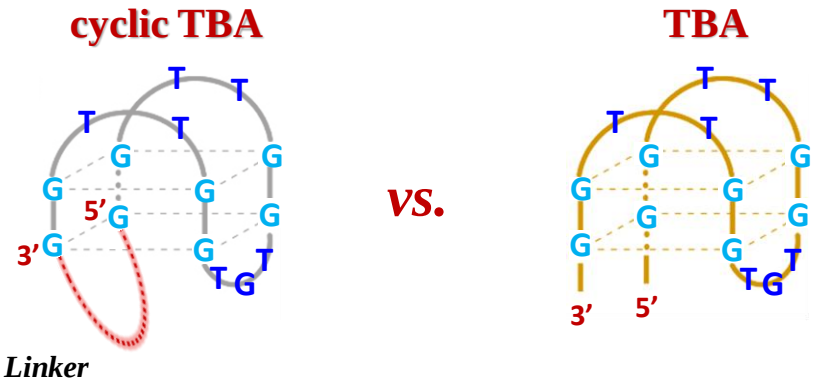

https://doi.org/10.1016/j.bioorg.2019.103379

Figure 1. Schematic representation of a cyclic TBA structure - with a linker connecting the 3′- and 5′-ends of the oligonucleotide sequence - compared to the antiparallel G-quadruplex structure formed in solution by unmodified TBA.

The biophysical characterization of this first cyclic TBA prototype, that we named cycTBA, highlighted the noteworthy advantages obtained upon cyclization of the aptamer: indeed, a remarkable increase in the thermal stability of its G-quadruplex structure (ΔT_m of ca. + 18 °C in both the analysed K^+- and Na^+-rich buffer solutions) and a dramatically higher resistance to nuclease degradation (ca. 180-fold higher half-life in PBS) were observed, denoting a much more compact and tightly assembled structure compared to unmodified TBA.[42] This cyclic TBA analogue was obtained by covalently linking the 3′- and 5′-ends of the TBA sequence (Figure 1), which in the folded antiparallel G4 structure point in the same direction and are far away from the TT loops recognized by the protein.[43–45] Thus, the presence of a circularizing linker in principle should not impair the recognition and interaction of the aptamer with the target protein.

Anyhow, its anticoagulant activity - determined by dynamic light scattering (DLS) analysis in phosphate buffer solutions (PBS) of fibrinogen in the presence of human α-thrombin - was ca. 50 % that of unmodified TBA, also correlated with a ca. halved binding affinity to thrombin.[42] These data can be rationalized considering that some mutual interactions between the aptamer and the protein occur which are definitively responsible for TBA bioactivity, as suggested also by other research groups.[9,45] In this frame, the increased rigidity of the G4 structure of TBA produced by cyclization, if over a certain limit, could somehow reduce its affinity for the protein, and thus its bioactivity.

However, the overall results obtained on the first cyclic TBA prototype - clearly demonstrating the favourable impact of cyclization on the biophysical features of TBA - proved that there is significant room for improvement, particularly by finely tuning the design of the connecting linker. This structural component can indeed be optimized to realize the best compromise between pre-organizing/stabilizing the TBA G4 structure, necessary for thrombin recognition, and maintaining some structural flexibility degrees, so to achieve an improved target affinity and bioactivity.

Stimulated by our previous study, we here report the design, synthesis and characterization of a small library of novel cyclic TBA analogues, indicated as cycTBAs **I**-**IV** (Table 1), differing for the linker connecting the TBA ends. In particular, these novel analogues exhibit flexible linkers with increased length with respect to the previously reported cycTBA, which should provide a still compact, stable G4 core, however allowing higher structural flexibility compared to their precursor.

In particular, cycTBA **I** and **II** were obtained using a chemical cyclization strategy based on the oxime ligation method,[46,47] while cycTBA **III** and **IV** were circularized using a Cu(I)-assisted azide-alkyne cycloaddition (CuAAC) protocol,[48] also adopted to obtain our first prototype,

https://doi.org/10.1016/j.bioorg.2019.103379

cycTBA.[42] More in detail, cycTBA **I** was prepared also to evaluate whether the oxime ligation approach was more efficient, in terms of cyclization yields, than the alternative, previously explored CuAAC. Therefore, cycTBA **I** was designed with a linker only slightly longer than the one used in cycTBA (22- vs. 20-atom length). In turn, in cycTBA **II** one triethylene glycol unit - a flexible linker typically used in bioconjugation strategies - was inserted at each end, providing a 30-atom long linker. Then, cycTBA **III** and **IV** were prepared using the CuAAC protocol, analogously to cycTBA,[42] introducing one or two tetraethylene glycol units, thus producing connecting linkers 34- and 48-atom long, respectively (Table 1).

The exploited synthetic strategies allowed obtaining circularizing linkers varying not only in length but also featuring marked differences in their chemical structure.

With this second generation of cyclic TBAs, we intended to improve the potency of TBA in inhibiting fibrin clot formation, aiming at obtaining suitable derivatives concomitantly featuring increased thermal stability and nuclease resistance. Then, as additional goal, we intended to evaluate the cyclization approach from a synthetic point of view, probing the chemical scope of the different cyclization reactions, with special attention to the yield optimization, as well as from a functional point of view, analysing the impact of the length and chemical nature of the linker on the TBA performance. In this frame, our studies were also aimed at identifying the structural elements more effective for TBA cyclization in order to extend this strategy to other G4-based aptamers of great biological interest, involved in clotting disorders but also in other pathologies, such as cancer.

Name	Linker connecting sequence (5'-3')	Linker connecting length
cycTBA	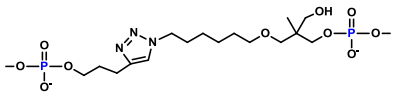	**20 atoms**
cycTBA I	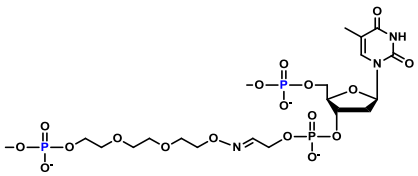	**22 atoms**
cycTBA II	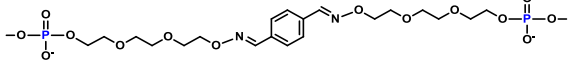	**30 atoms**
cycTBA III	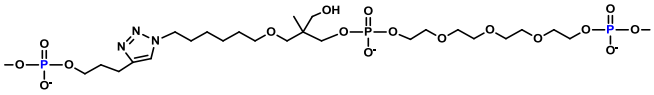	**34 atoms**
cycTBA IV	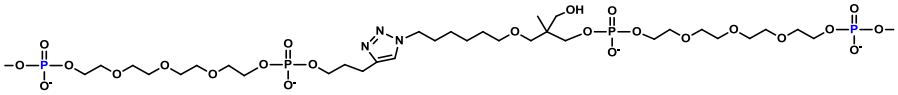	**48 atoms**

Table 1. Molecular structure and length of the linkers connecting the 3′- and 5′-ends of TBA, providing the new cycTBAs **I-IV**, here investigated. In the Table, the previously studied cycTBA[42] is also reported for comparison.

By using several biophysical techniques, the influence of the different inserted linkers on the conformational behaviour, thermodynamic stability, nuclease resistance and anticoagulant activity of cycTBAs **I-IV** was here analysed.

In particular, the novel cyclic analogues were studied, in comparison with the unmodified TBA, by UV, CD, CD-melting, gel electrophoresis and SE-HPLC techniques. In order to evaluate the effects of different saline conditions on the structuring ability of these aptamers, all these investigations were carried out in two different phosphate buffer solutions, containing a high content of K^+ (10 mM KH_2PO_4/K_2HPO_4, 70 mM KCl, 0.2 mM EDTA, pH 6.9, here indicated as K^+-rich buffer) or of Na^+ (*i.e.* PBS: 137 mM NaCl, 2.7 mM KCl, 10 mM NaH_2PO_4/Na_2HPO_4, 1.8 mM KH_2PO_4/K_2HPO_4, pH 7.0, here indicated as Na^+-rich buffer), respectively mimicking the intra- and extracellular environment.

In addition, the anticoagulant activity of these cyclic oligonucleotides compared to that of unmodified TBA was determined by dynamic light scattering (DLS) measurements in PBS (Na^+-rich buffer), which mimes the blood salt composition and is indeed relevant from a biological point of view.

2. EXPERIMENTAL SECTION

2.1. General methods. All the reagents and solvents were of the highest commercially available quality and were used as received. Acrylamide, GelRed Nucleic Acid Stain, and Tris-Borate-EDTA (TBE) 10X were purchased from VWR. Ammonium persulfate (APS), tetramethylethylenediamine (TEMED), Fetal Bovine Serum (FBS) were purchased from Sigma Aldrich.

The solid support **12** and the pentynyl phosphoramidite **13**[48] were synthesized according to reported protocols. Tetraethylene glycol phosphoramidite is commercially available from ChemGenes.

RP-HPLC analyses were performed at 60 °C on a Macherey Nagel Nucleodur 100−3 C 18 ec column (length: 75 mm, ID: 4.6 mm), using a linear gradient of B (0 to 30 %) in A for 20 min at 1 mL min^{-1}. Solution A: 1 % CH_3CN/0.05 M TEAA, solution B: 80 % CH_3CN/0.05 M TEAA.

MALDI-TOF MS studies were performed on a Shimadzu Assurance equipped with a 337 nm nitrogen laser. Spectra were recorded in negative ion mode, using 2,4,6-trihydroxyacetophenone (THAP) with 10 % ammonium citrate as a matrix in H_2O/CH_3CN, 1:1, v/v. Aqueous sample solutions were mixed with the matrix as 1:1 or 1:5 v/v ratio and 1 µL of the solution was then deposited on the stainless steel plate for drying.

2.2. Synthetic procedures

Monomethoxytritylaminooxytriethyleneglycol 3. Hydrazine hydrate (437 µL, 9.0 mmol) was added to a solution of phthalimide triethyleneglycol **1**[47] (970 mg, 3.28 mmol) in pyridine (14 mL). The reaction, left under stirring, produced a white precipitate already after 5 min. After 1 h, this precipitate was removed by filtration and the solution was then co-evaporated three times with anhydrous pyridine. Crude compound **2** was dissolved in anhydrous pyridine (26 mL) at 0 °C, and then MMTrCl (1.g, 3.2 mmol) was added in three aliquots over 30 min. The solution was stirred at r.t. for 2.5 h and then methanol (1 mL) was added. After 5 min the solution was diluted with CH_2Cl_2 (50 mL) and washed with saturated $NaHCO_3$ aqueous solution (50 mL) after extraction with CH_2Cl_2 (2 x 50 mL). The organic layers were then dried over anhydrous Na_2SO_4 and taken to dryness. The crude was purified by flash chromatography on a silica gel column eluted with a gradient from 0 to 50 % of ethyl acetate in cyclohexane containing 1 % TEA, which afforded compound **3** in 67 % isolated yields (980 mg).

^{1}H NMR ($CDCl_3$, 400 MHz, Figure S1a): δ 2.31 (1H, OH), 3.41-3.58 (10H, CH_2OH, O-CH_2-CH_2-O), 3.71-3.76 (5H, CH_3O, NO-CH_2), 6.72-6.75 (2H, Ar), 6.51 (1H, NH), 7.12-7.25 (12H, Ar).

^{13}C MR ($CDCl_3$, 100 MHz, Figure S1b): δ 55.2, 61.8, 69.7, 70.4, 70.5, 72.5, 73.2, 73.5, 113.0, 126.8, 127.6, 129.1, 130.4, 136.6, 144.7, 158.3.

HRMS (ESI/Q-TOF): $[M + H]^+$ calc. for $C_{26}H_{32}NO_5$ 438.2280, found 438.2276.

Monomethoxytritylaminooxytriethyleneglycol 2-cyanoethyl *N*,*N*-diisopropyl-phosphoramidite 4. Compound **3** (650 mg, 1.5 mmol) was coevaporated twice with anhydrous acetonitrile and then dissolved in anhydrous CH_2Cl_2 (10 mL). Anhydrous diisopropylethylamine (DIEA, 325 µL, 1.8 mmol) and 2-cyanoethyl-*N*,*N*-diisopropylphosphoramidochloridite (330 µL, 1.5 mmol) were then added to the compound **3** solution under argon atmosphere. After 30 min under stirring, water (0.5 mL) was added and the organic phase was washed with saturated aqueous $NaHCO_3$ (70 mL) and extracted with CH_2Cl_2 (2 x 50 mL). The organic layer was then dried over anhydrous Na_2SO_4 and taken to dryness. The crude was purified by silica gel chromatography (cyclohexane/AcOEt/ with 4 % TEA) from 1:0 to 7:3 to afford pure phosphoramidite **4** in 87 % overall yields (823 mg).

^{1}H NMR ($CDCl_3$, 300 MHz, Figure S2a): δ 1.11-1.16 (12H, $NiPr_2$), 2.54-2.59 (2H, CH_2CN), 3.44-3.80 (19H, CH_2OP, O-CH_2-CH_2-O, N-O-CH_2, CH_3O, N-CH), 6.50 (1H, NH), 6.75-6.78 (2H, Ar), 7.16-7.28 (12H, Ar).

^{13}C NMR ($CDCl_3$, 100 MHz, Figure S2b): δ 19.2, 23.5, 23.6, 23.7, 42.1, 54.2, 57.5, 61.5, 68.7, 69.4, 69.6, 70.1, 72.1, 72.5, 111.9, 116.7, 125.7, 126.6, 128.1, 129.3, 135.6, 143.7, 157.3.

^{31}P NMR ($CDCl_3$, 121 MHz, Figure S2c): δ 148.6.

HRMS (ESI/Q-TOF): $[M + H]^+$ = calc. for $C_{35}H_{49}N_3O_6P$ 638.3359, found 638.3351.

Synthesis of the unmodified TBA. TBA was synthesized according to reported protocols[42] by using commercially available CPG solid support and base-protected 2-cyanoethyl, *N*,*N*-diisopropylphosphoramidite monomers and exploiting standard phosphoramidite chemistry. Analytical RP-HPLC retention time: 9.81 min, MALDI-TOF MS: m/z: $[M-H]^-$: for $C_{150}H_{186}N_{57}O_{94}P_{14}$ calc.: 4725.04; found: 4725.70.[42]

Synthesis of cyclic TBA derivatives. The TBA sequence was elongated from commercially available glycerol-derivatized solid support **5**, levulinoyl-derivatized solid support **9**[49] or azide-derivatized support **12**[48] on an ABI 394 DNA synthesizer, with a 1 μmol scale cycle, according to standard phosphoramidite chemistry protocols. The detritylation step was performed for 65 s using 3 % TCA in CH_2Cl_2. For the coupling step: benzylmercaptotetrazole (0.3 M in anhydrous CH_3CN) was used as the activator with commercially available thymidine or N^2-*i*Bu or N^2-*t*BuPac- 2′-deoxyguanosine-2-cyanoethyl, *N*,*N*-diisopropylphosphoramidite (0.075 M in CH_3CN, 30 s coupling time), MMTrN-EG_3 phosphoramidite **4** (0.1 M in CH_3CN, 60 s coupling time), DMTr-EG_4-phosphoramidite (0.1 M in CH_3CN, 60 s coupling time) or pent-4-yn-1-yl phosphoramidite **13**[48] (0.1 M in CH_3CN, 60 s coupling time). The capping step was performed with acetic or phenoxyacetic (Pac) anhydride using commercially available solutions (Cap A: acetic anhydride:pyridine:THF 10:10:80 v/v/v and Cap B: 10 % *N*-methylimidazole in THF) for 10 s or Cap A: Pac anhydride:pyridine:THF 10:10:80 v/v/v and Cap B: 10 % *N*-methylimidazole in THF) for 60 s. The oxidation step was performed with a standard, diluted iodine solution (0.1 M I_2, THF:pyridine:water 90:5:5, v/v/v) for 15 s.

Cyclization by oxime ligation (cycTBA I). Solid-supported oligonucleotide **6** was introduced into a sealed vial and treated with concentrated aqueous ammonia (2 mL) for 5 h at 55 °C. After evaporation, the resulting linear oligonucleotide **7** was purified by HPLC (189 nmol). Analytical RP-HPLC retention time: 11.95 min, MALDI-TOF MS: m/z: $[M-H]^-$ = calc. 5682.83, found 5683.77.

Then 50 mM KCl (400 μL) and 100 mM $NaIO_4$ (5 μL) were added to a solution of **7** in water (100 μL). After 2 h, formaldehyde was removed by evaporation (speedvac) and 400 μL of 0.4 M NH_4Ac buffer (pH = 4.2) were added. The resulting cycTBA **I** was purified by HPLC affording 74 nmol of the target compound (40 % isolated yields). Analytical RP-HPLC retention time: 10.08 min, MALDI-TOF MS: m/z: $[M-H]^-$ = calc. 5360.42, found 5360.74.

Cyclization by bis-oxime ligation (**cycTBA II).** Solid-supported oligonucleotide **10** was treated with a 7 M ammonia solution in methanol at r.t. for 3 h. After washings with methanol, the CPG beads were transferred into a vial and treated with a 50 mM CH_3ONH_2 HCl solution in 0.4 M NH_4Ac buffer, pH = 4.2 (2 mL) for 2 h at r.t. The linear TBA **11** was purified by size exclusion

chromatography cartridges (NAP-10), recovering 320 nmol of the target compound which were then lyophilized. Analytical RP-HPLC retention time: 11.56 min, MALDI-TOF MS: m/z: [M-2H + NH_4^+]$^-$ = calc. 5196.41, found 5197.78.

The crude was dissolved in water (120 µL) and then 50 mM KCl (500 µL), 0.4 M NH_4Ac buffer pH = 4.2 (3.0 mL) and 360 nmol of terephthalaldehyde (10 mM in methanol, 36 µL) were sequentially added. After 3 h at r.t., the crude was purified by size exclusion chromatography cartridges (NAP-25) affording cycTBA **II** in 58 % overall yields (186 nmol). Analytical RP-HPLC retention time: 13.42 and 13.75 min for E/Z isomers,[47] MALDI-TOF MS: m/z: $[M-H]^-$ = calc. 5277.49, found 5278.83.

Cyclization by CuAAC (**cycTBAs III and IV).** Oligonucleotide-functionalised CPG beads **16** and **17** were introduced into a sealed vial and treated with concentrated aqueous ammonia (2 mL) overnight at 40 °C. The supernatant was withdrawn and evaporated. The linear modified TBAs **16** and **17** were dissolved in water and then analyzed by UV, HPLC and MALDI-TOF MS. The amount of crude **16** and **17**, determined by UV measurements at 260 nm, was 0.93 and 0.95 µmol, respectively.

16: Analytical RP-HPLC retention time: 16.69 min, MALDI-TOF MS: m/z: $[M-H]^-$ = calc. 5434.64, found 5433.21.

17: Analytical RP-HPLC retention time: 16.89 min, MALDI-TOF MS: m/z: $[M-H]^-$ = calc. 5690.83, found 5691.92.

Protocol for TBA cyclization. Freshly prepared, 100 mM aq. solutions of $CuSO_4$ (5 eq, 5 µmol, 50 µL) and 500 mM sodium ascorbate (10 eq, 10 µmol, 40 µL), were added to a solution of linear TBA **16** (0.93 µmol) or **17** (0.95 µmol) dissolved in 1 mL of H_2O and KCl (50 mM, 4 mL). The vials containing the resulting mixture were sealed and stirred at r.t. After 1 h, the mixtures were purified by size exclusion chromatography (SEC) on a NAP-25 column (GE-Healthcare), giving crude compounds cycTBAs **III** and **IV,** which were frozen and lyophilized. The crudes were then purified by HPLC affording cycTBA **III** (255 nmol, 27 % overall yields, analytical RP-HPLC retention time: 12.66 min, MALDI-TOF MS: m/z: $[M-H]^-$ = calc. 5434.64, found 5435.67) and cycTBA **IV** (350 nmol, 37 % overall yields, analytical RP-HPLC retention time: 13.14 min, MALDI-TOF MS: m/z: $[M-H]^-$ = calc. 5690.83, found 5690.92) which were frozen and lyophilized.

2.3. Preparation of the oligonucleotide samples. Purified and lyophilized TBA and cyclic TBAs oligonucleotides (here named as cycTBA **I**, cycTBA **II**, cycTBA **III** and cycTBA **IV**, Table 1) were dissolved in a defined volume of Milli-Q water. Their concentrations were determined by UV measurements on a JASCO V-530 UV-vis spectrophotometer equipped with a Peltier Thermostat JASCO ETC-505T, using a 1 cm path length cuvette (1 mL internal volume, Hellma), recording the

absorbance at 260 nm and 90 °C. The molar extinction coefficient of 158.480 cm^{-1} M^{-1} was used for both TBA and the cyclic TBAs (assuming negligible for the latter ones the contribution of the linkers at 260 nm), as calculated for the unstacked oligonucleotides. The UV spectra were recorded in the range 200–320 nm with a medium response, a scanning speed of 100 nm/min and a 2.0 nm bandwidth with the appropriate baseline subtracted. Taking a suitable aliquot from the initial stock solutions in H_2O, all the investigated oligonucleotides were then diluted in the selected K^+- (10 mM KH_2PO_4/K_2HPO_4, 70 mM KCl, 0.2 mM EDTA, pH = 6.9) or Na^+-rich (PBS: 137 mM NaCl, 2.7 mM KCl, 10 mM NaH_2PO_4/Na_2HPO_4, 1.8 mM KH_2PO_4/K_2HPO_4 pH = 7.0) phosphate buffer solutions. Thereafter, the samples were annealed by heating the solutions for 5 min at 95 °C and then allowed slowly cooling to r.t. overnight. The annealed samples were eventually kept at 4 °C until their subsequent use.

2.4. UV Thermal Difference Spectra. The UV spectra measurements were performed on a JASCO V-530 UV-vis spectrophotometer equipped with a Peltier Thermostat JASCO ETC-505T, using 1 cm path length cuvette (1 mL internal volume, Hellma). cycTBAs **I-IV** were dissolved in the selected buffer so to obtain 2 μM solutions and annealed. The absorbance spectra were recorded at 15 and 90 °C in the range 200-320 nm using a scanning speed of 100 nm/min with the appropriate baseline subtracted. The thermal difference spectra (TDS) were obtained by subtracting the UV spectrum recorded at a temperature below the T_m (15 °C), at which the aptamer is fully structured, from the one obtained at a temperature above the T_m (90 °C), where the oligonucleotide G4 structure is fully denatured.[50–52] Each experiment was performed in triplicate.

2.5. Circular dichroism (CD) spectroscopy. CD spectra and CD-monitored melting curves were recorded on a Jasco J-715 spectropolarimeter equipped with a Peltier-type temperature control system (model PTC-348WI), using a quartz cuvette with a path length of 1 cm (3 mL internal volume, Hellma). CD parameters for spectra recording were the following: spectral window 220–320 nm, data pitch 1 nm, band width 2 nm, response 4 s, scanning speed 100 nm/min, 3 accumulations. cycTBAs **I-IV** were analysed at 2 μM concentration in the selected buffers. Thermal denaturation-renaturation curves were recorded following the CD signal at 295 nm vs. the temperature (scan rate 1.0 °C/min) and recording spectra from 220 to 320 nm in 5 °C steps, in the 20 - 90 °C temperature range for both the K^+- and Na^+-rich buffer solutions. Each experiment was performed in triplicate. The molar ellipticity [θ] (deg cm^2 $dmol^{-1}$) was calculated from the equation $[\theta] = \theta_{obs}/10 \times l \times C$, where θ_{obs} is the observed ellipticity (mdeg), C is the oligonucleotide molar concentration, and l is the optical path length of the cell (cm). Data were also converted into folded fraction (α) calculated as: $\alpha = [\theta(T) - \theta_U)/(\theta_F - \theta_U)]$, where θ(T) is the molar ellipticity at 295 nm at each temperature, while θ_F and θ_U are the molar ellipticity at 295 nm for the folded (T = 20 °C) and

unfolded (T = 90 °C) oligonucleotide, respectively. The T_m values were estimated as the maxima of the first derivative plots of the melting/annealing curves and the error associated with the T_m determination was ± 1 °C. The ΔT_m, values were calculated by subtracting the measured T_m of unmodified TBA from that observed for each cyclic TBA analogue. The CD melting curves showed sigmoidal profiles and were also modelled by a two-state transition, using a theoretical equation for an intramolecular association, according to the van't Hoff analysis.[51,53] Thermodynamic data were obtained using the following equations:

$$\theta_u(T) = \theta_u^0 + m_u*T$$

$$\theta_l(T) = \theta_l^0 + m_l*T$$

$$\alpha = [\theta(T) - \theta_l(T)]/[\theta_u(T) - \theta_l(T)]$$

$$\theta(T) = \alpha* [(\theta_u^0 + m_u*T) - \theta_l^0 + m_l*T] + (\theta_l^0 + m_l*T)$$

$$\alpha = K_a/(1 + K_a)$$

$$K_a = \exp(\Delta H_{v.H}/RT)*[(T/T_m) - 1]$$

where:

θ_u and θ_l are linear equations describing the upper and lower baselines, respectively, θ_u^0 and θ_l^0 are fitted parameters for the intercepts of the upper and lower baseline, while m_u and m_l are the respective slopes. θ(T) is the dependent variable and is the experimentally determined molar ellipticity (θ) at each temperature (T). K_a is the equilibrium constant for the unstructured → structured oligonucleotide transition for an intramolecular process and α is the folded fraction.

Using these equations, T_m and $\Delta H_{v.H}$ change values of the unfolding processes were calculated and the reported results provided the best fit of the experimental melting data. The $\Delta S_{v.H}$ values were calculated by equation $\Delta S_{v.H} = \Delta H_{v.H}/T_m$. and free energy change values (at 298 K) by the equation $\Delta G_{v.H} = \Delta H_{v.H} - T\Delta S_{v.H}$. All the thermodynamic parameters are expressed in kJ/mol with the corresponding errors within ± 10 %.

2.6. Non-denaturing polyacrylamide gel electrophoresis (PAGE). Slowly annealed samples of unmodified TBA and cycTBAs **I-IV** dissolved at 20 μM concentration in both the selected K^+- and Na^+-rich buffer solutions were loaded on 15 % polyacrylamide gels in TBE (Tris-Borate-EDTA, 0.5X) as running buffer. All the samples were supplemented with 5 % glycerol just before loading and then run, under native conditions, at 100 V at r.t. for 75 min. Gels were stained with a GelRed solution (supplemented with NaCl 0.1 M) for 20 min and finally visualized with a UV transilluminator (BioRad ChemiDoc XRS). Each experiment was performed in triplicate.

2.7. Size exclusion chromatography. SE-HPLC analyses were performed using an Agilent HPLC system, equipped with a UV/vis detector, on a Yarra 3 μm analytical column (300 x 4.60 mm;

Phenomenex). The elution was monitored at λ = 254 nm with 0.35 mL min^{-1} flow rate. The mobile phases consisted of the K^+- (10 mM KH_2PO_4/K_2HPO_4, 70 mM KCl, 0.2 mM EDTA, pH = 6.9) or Na^+-rich (PBS: 137 mM NaCl, 2.7 mM KCl, 10 mM NaH_2PO_4/Na_2HPO_4, 1.8 mM KH_2PO_4/K_2HPO_4, pH = 7.0) buffer solutions. cycTBAs **I-IV** were investigated at 2 μM concentration in the selected buffer solution and slowly annealed before the HPLC analysis. The error associated with the retention time (t_R) determination is within ±5 %.

2.8. Enzymatic stability assays by Nucleogen-SAX HPLC analysis. The stability of cycTBAs **I-IV** in biological media was analysed by incubating the oligonucleotides - previously annealed in PBS buffer - at 10 μM concentration in 80 % of fetal bovine serum (FBS) at 37 °C. Then, at fixed times, 20 μL of the samples were collected, inactivated at 95 °C for 3 min and finally stored at -20 °C until their analysis. These aliquots were then diluted to 100 μL with solution A (20 mM KH_2PO_4 aq. solution, pH 6.9, containing 20 % (v/v) CH_3CN), filtered on 0.2 μm filter and finally analysed by HPLC. For these experiments, a Nucleogen DEAE 60-7 column (Macherey-Nagel, 7 μm, 125 x 4 mm) with a flow rate of 0.8 mL min^{-1}, detection at 254 nm and a linear gradient of B (0 to 100 %) in A in 30 min was used, until disappearance of the peak attributed to the intact oligonucleotide. Solution A: 20 mM KH_2PO_4/K_2HPO_4 aq. solution, pH 6.9, containing 20 % (v/v) CH_3CN; solution B: 1 M KCl, 20 mM KH_2PO_4/K_2HPO_4 aq. solution, pH 7.0, containing 20 % (v/v) CH_3CN. Each experiment was performed at least in triplicate. The oligonucleotide area under the peak, at each collected time, was then calculated and normalized with respect to the initial one. Percentages of the remaining area are reported as mean values ± SD for multiple determinations. Half-life times of each aptamer ($t_{1/2}$) was obtained by fitting the values with an equation for kinetics of one order.

2.9. Anticoagulant activity by light scattering measurements. Evaluation of the anticoagulant activity of cycTBAs **I-IV** and unmodified TBA, used as control, was performed by means of light scattering (LS) experiments analysing the normalized autocorrelation functions, which give information on the size of the species in the system at a certain time, and monitoring the increase of the light scattered intensity upon conversion of fibrinogen to fibrin catalysed by thrombin.[31] A 1.2 μM solution of fibrinogen in PBS was placed in a LS cuvette and left to equilibrate in the instrument for 20 min. Then, thrombin was added up to a final concentration of 5 nM and the light scattered intensity was registered every 20 s for at least 2 h. Experiments with the different aptamers were performed by adding each oligonucleotide, previously annealed in PBS, to the fibrinogen solutions before addition of thrombin at a concentration providing a thrombin:oligonucleotide molar ratio of 1:5. All the experiments were performed at least in triplicate.

By plotting the normalized scattered intensity nI

https://doi.org/10.1016/j.bioorg.2019.103379

$$nI = (I-I_0)/I_0$$

where I is the scattered intensity at time t and I_0 the scattered intensity at t=0, as a function of time and by linearly fitting the initial increase of nI upon the lag time, it is possible to obtain an estimation of the coagulation rate from the slopes of the fitted lines. The thrombin inhibiting properties of the different oligonucleotides were then compared by calculating the anticoagulant efficacy as the ratio between the coagulation rate in the exclusive presence of thrombin and in the concomitant presence of thrombin and aptamers.[45]

3. RESULTS AND DISCUSSION

3.1. Synthetic procedures for the preparation of cyclic TBA variants

Four different cyclic TBA analogues - exhibiting linkers of different length between the 3′ and 5′ terminal 2′-deoxyguanosines of the TBA sequence (Table 1) - were successfully synthesized and characterized. The cyclic TBAs indicated as cycTBA **I** and cycTBA **II**, with a 22- and 30-atom linker, were respectively prepared by using oxime[46] and bis-oxime[47] ligation procedure; while cycTBA **III** and cycTBA **IV**, with a 34- and 48-atom linker, respectively, were obtained by CuAAC.[42,48]

cycTBA **I** was synthesized according to the strategy developed by Dumy et al.[46], exploiting the oxime ligation between an oxyamine linker introduced at the 5′-end and an aldehyde function generated by oxidation of a 3′-glycerol moiety (Scheme 2). To this end, we first synthesized the monomethoxytrityl-aminooxytriethyleneglycol phosphoramidite **4** starting from phthalimidotriethyleneglycol **1**[47] (Scheme 1). The phthalimide group was removed by hydrazine treatment and the resulting aminooxy function was then protected with the MMTr group to provide compound **3**, finally phosphitylated to give phosphoramidite **4**. The identity of compounds **3** and **4** was confirmed by NMR and MS analyses (Figures S1 and S2).

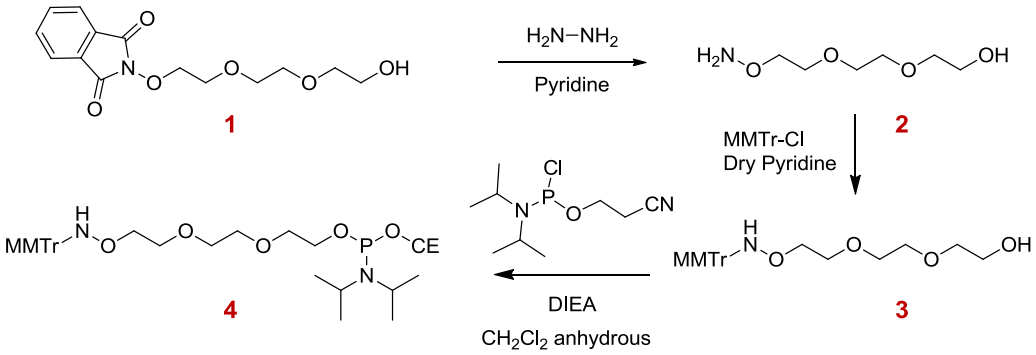

Scheme 1. Synthesis of MMTr-aminooxytriethyleneglycol phosphoramidite **4**.

https://doi.org/10.1016/j.bioorg.2019.103379

Thus, starting from the commercially available glycerol-derivatized solid support **5**, the TBA oligonucleotide sequence was elongated and **4** was coupled at its 5′-end using standard phosphoramidite chemistry. After ammonia treatment on **6**, the 3′-glycerol-derivatized oligonucleotide **7** was dissolved in a KCl aq. solution to allow its G-quadruplex folding, and the glycerol moiety at the 3′-end was oxidized to the aldehyde derivative **8**. After removal of the obtained formaldehyde by evaporation, the residue was dissolved in ammonium acetate buffer to deprotect the 5′-aminooxy function and allow its coupling with the 3′-aldehyde to form the target cyclic TBA by oxime ligation. The resulting cycTBA **I** was then purified by HPLC and characterized by MALDI-TOF MS analysis (Figure S3).

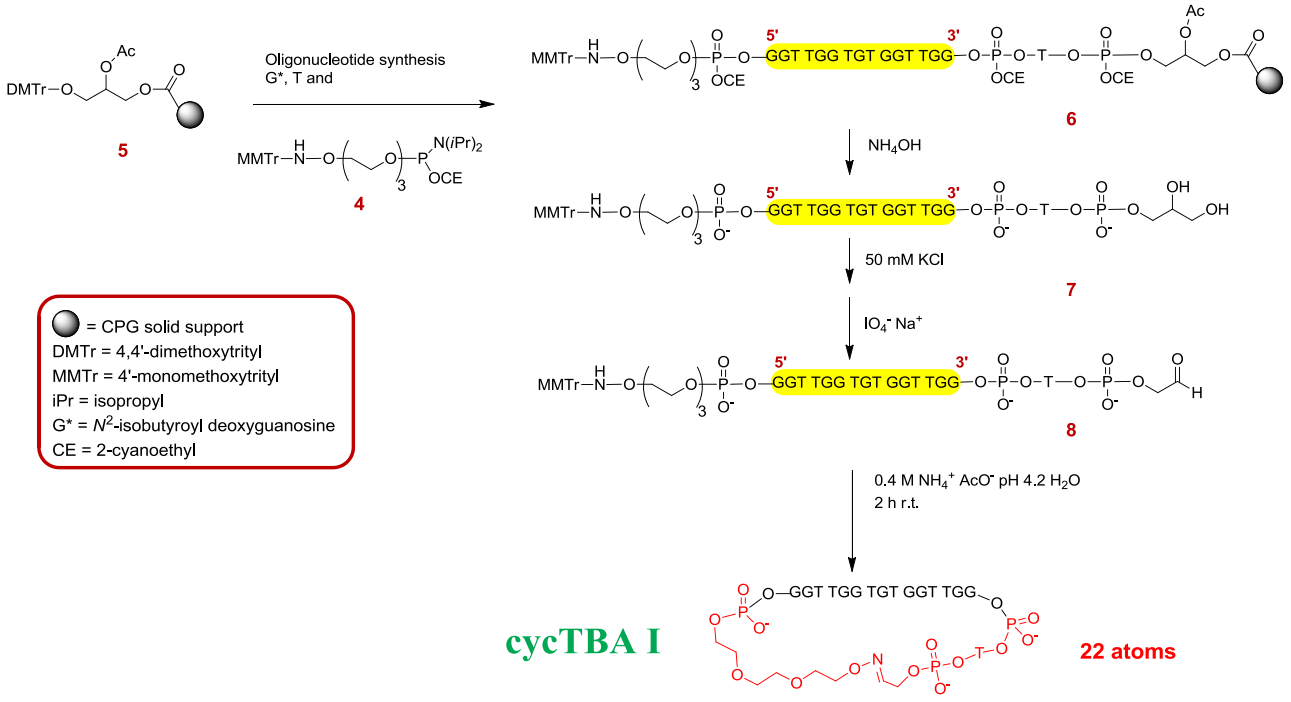

Scheme 2. Synthetic scheme for the preparation of cycTBA **I** by oxime ligation.

For the synthesis of cycTBA **II**, a bis-oxime ligation[47] protocol (Scheme 3) was applied exploiting a strategy recently reported by some of us. Starting from solid support **9**,[49] the TBA sequence was elongated, using *t*Bu-phenoxyacetyl (*t*Bu-Pac) protection for the 2′-deoxyguanosine building blocks, and then compound **4** was coupled. The resulting support-bound oligonucleotide **10** was treated first with ammonia solution in methanol, to remove the 2-cyanoethyl and *t*Bu-Pac groups, and then with methoxyamine HCl in ammonium acetate buffer, to obtain its detachment from the solid support and the MMTr removal, affording the linear 3′,5′-bis aminooxy-TBA **11**. After size exclusion chromatography, linear oligonucleotide **11** was circularized by addition of

https://doi.org/10.1016/j.bioorg.2019.103379

terephthalaldehyde and KCl to give cycTBA **II,** then purified by HPLC and characterized by MALDI-TOF MS analysis (Figure S4).

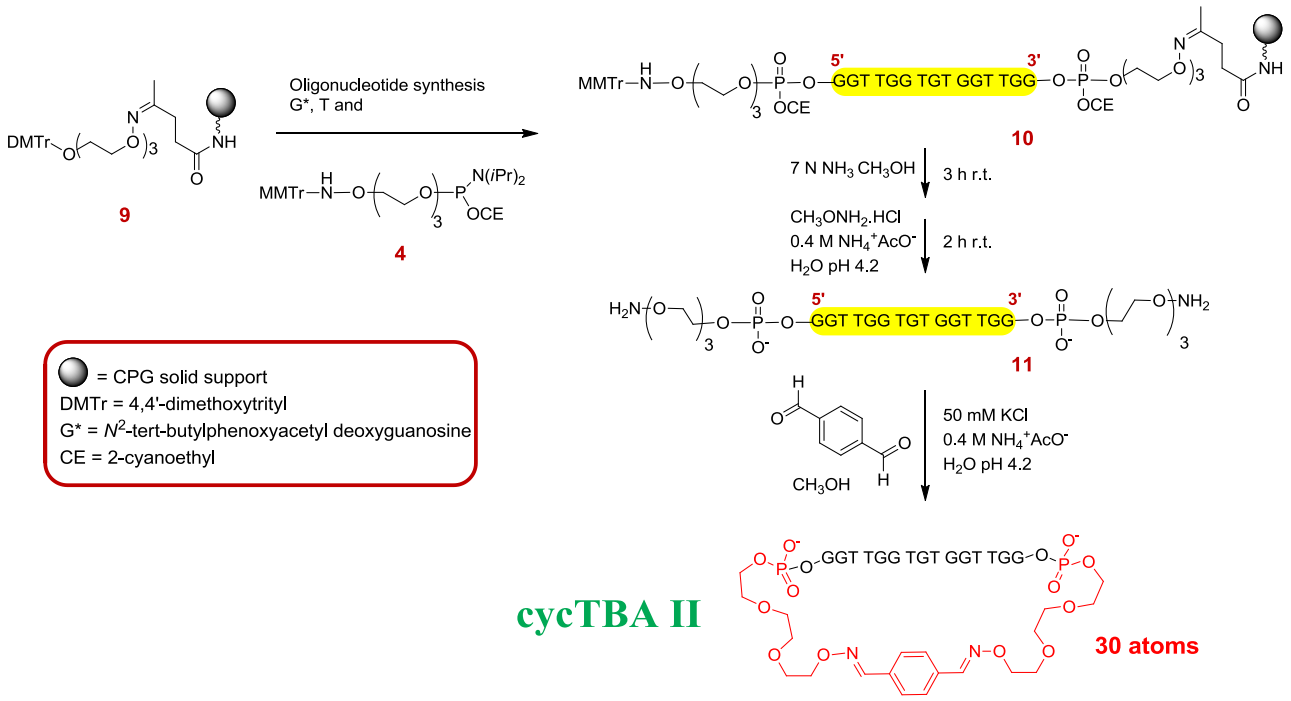

Scheme 3. Synthetic scheme for the preparation of cycTBA **II** by bis-oxime ligation.

As concerning the synthesis of cycTBAs **III** and **IV**, respectively exhibiting a linker of 34 and 48 atoms between the two 3′ and 5′-terminal 2′-deoxyguanosines (Table 1), CuAAC protocols were exploited, analogously to the previously developed cycTBA precursor.[42]

In detail, these cyclic TBA analogues were synthesized starting from the azido-functionalised solid support **12**[48] (Scheme 4). In the case of cycTBA **III**, a tetraethyleneglycol (EG_4) spacer was introduced before the oligonucleotide sequence elongation - using standard phosphoramidite chemistry - and then a pentynyl group[48] was inserted at the 5′-end by reaction with phosphoramidite **13**. In the case of cycTBA **IV**, an additional EG_4 spacer was introduced after the oligonucleotide assembly, followed by coupling with the pentynyl phosphoramidite **13** (Scheme 4). Then, support-bound oligonucleotides **14** and **15** were fully deprotected and released in solution by ammonia treatment, affording the linear oligonucleotides **16** and **17**. Lastly, these were circularized by CuAAC, using $CuSO_4$ and sodium ascorbate in a K^+-containing solution, introduced to promote the oligonucleotide G-quadruplex folding and thus favour the spatial proximity of their 5′-and 3′-ends (Scheme 4). Resulting cycTBAs **III** and **IV** were purified by HPLC and then characterized by MALDI-TOF MS analysis (Figures S5 and S6).

https://doi.org/10.1016/j.bioorg.2019.103379

As previously observed,[42] in all cases the precursor linear oligonucleotides exhibited different retention times vs. their cyclic congeners by analytical RP-HPLC analysis, nicely confirming the effective cyclization (Figures S7-S10).

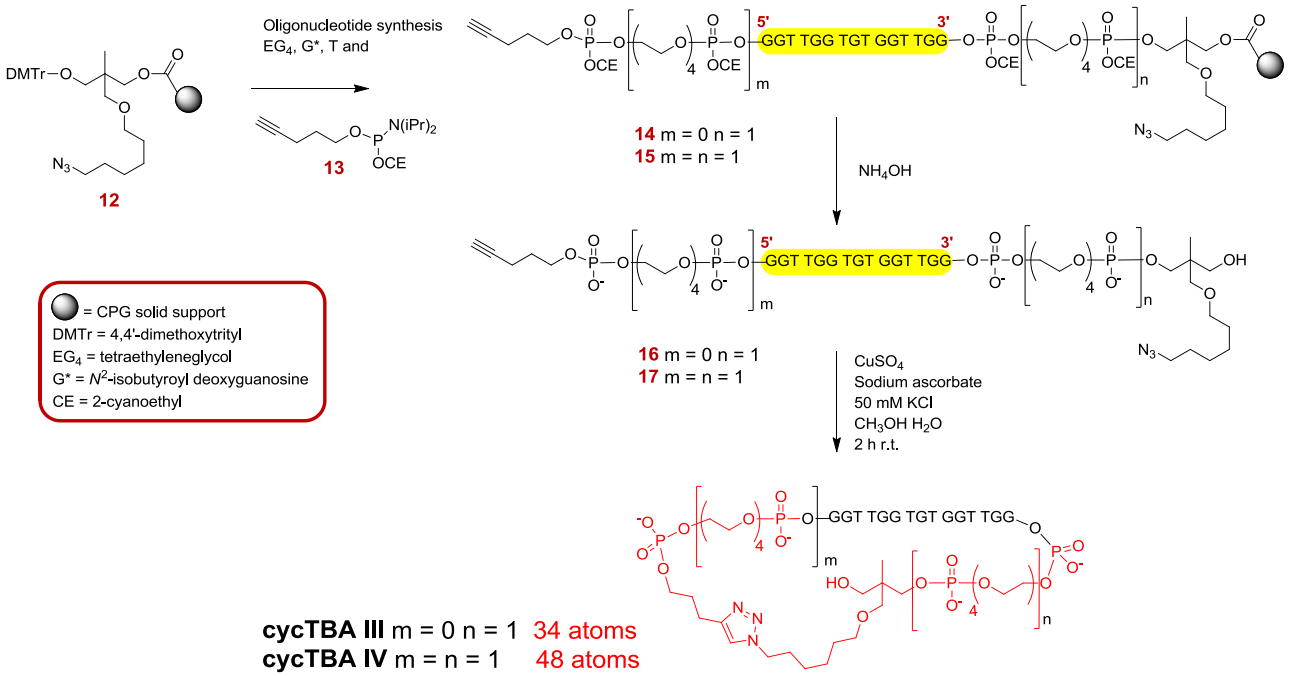

Scheme 4. Synthetic scheme for the preparation of cycTBAs **III** and **IV**.

3.2. Thermodynamic and spectroscopic features of cyclic TBA variants

3.2.1. UV spectra and TDS

The spectroscopic properties of cycTBAs **I-IV** were investigated by means of UV and CD spectroscopies in two different buffer solutions, containing a high content of K^+ or Na^+ ions, respectively. It is indeed well known that buffer composition, and particularly ion concentration, can determine dramatic changes in the biophysical properties[44,54–57] as well as in the anticoagulant activity of TBA, due to conformational changes involving key protein–aptamer interactions.[44]

For all the cyclic TBAs here investigated, UV thermal difference spectra (TDS) at 2 μM concentration were obtained recording spectra at low and high temperatures. Differential spectra - representing the spectral difference between the unfolded and the folded oligonucleotide - have a typical and unique shape for G-quadruplexes and can be used as a simple and rapid method to identify the presence of these structures in solution.[50–52] In Figures S11 and S12, the spectra at 15 and 90 °C (panels a and c) as well as the obtained TDS profiles (panels b and d) were reported for cycTBAs **I** and **II** as representative examples.

https://doi.org/10.1016/j.bioorg.2019.103379

All the UV spectra at 15 °C, in both saline solutions, revealed the characteristic absorption of TBA,[42] with the double-hump band between 230 and 300 nm (Figures S11 and S12). The obtained TDS profiles, in both K^+- and Na^+-rich solutions, showed for all the cyclic TBA analogues here investigated a positive band at 273 nm and a negative band at 295 nm, similarly to unmodified TBA,[42] providing the typical "fingerprint" of G-quadruplex structures (Figures S11 and S12).[50–52]

3.2.2. CD spectroscopy

In order to determine the effects of the circularizing linker on the conformational properties and thermal stability of the TBA G4 structure, CD spectra and CD thermal denaturation measurements were recorded for all the studied cyclic TBA analogues. The CD spectra at 15 °C of cycTBAs **I-IV**, at 2 μM concentration in both K^+- and Na^+-rich buffer solutions, are reported in Figure 2 in comparison with unmodified TBA, analysed under the same experimental conditions. These data nicely showed that all the novel analogues in both saline conditions folded into structures displaying a CD profile very similar to that of TBA, with only tiny differences in the profile or intensity of the bands (Figure 2).

In detail, for three of the here investigated cyclic TBAs (*i.e.* **I**, **III** and **IV**, orange, light blue and magenta lines, respectively), the recorded spectra are essentially superimposable to that of unmodified TBA showing two positive bands, with maxima at about 294-295 and 246-247 nm and one negative band with minima at 268-269 nm. These spectroscopic properties are fully consistent with an antiparallel G4 structure in which *anti* and *syn* guanosines alternate along the strands.[58–63]

Only in the case of cycTBA **II**, little changes in the CD spectra were observed (maxima and minima at 293 and 265 nm, in both saline conditions, together with the other maximum at 245/246 nm, respectively in K^+/Na^+ buffer solutions) corresponding to a slight shift in the minimum and in the maximum at low wavelengths (Figure 2), as already observed for the previously developed cycTBA.[42] Similar differences in the CD profiles of TBA analogues are not unprecedented[15] suggesting slight conformational differences in the G4 arrangement in solution.

https://doi.org/10.1016/j.bioorg.2019.103379

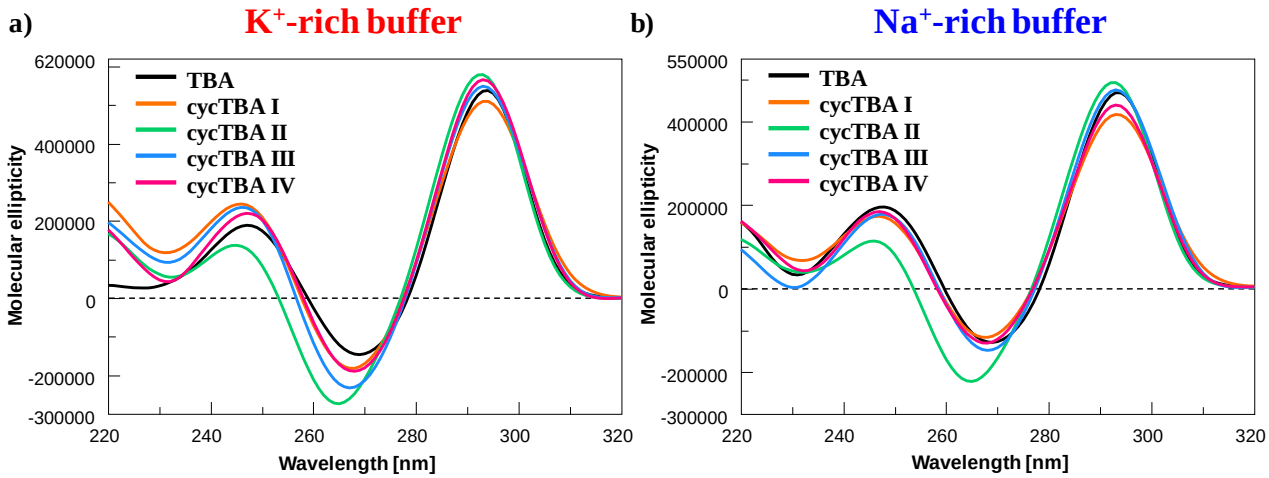

Figure 2. Overlapped CD spectra of cyclic TBAs **I-IV** (orange, green, light blue and magenta lines, respectively), recorded at 15 °C in both the selected K^+- (**a**) and Na^+-rich (**b**) buffer solutions, in comparison with unmodified TBA (black line). The investigated oligonucleotides were analyzed at 2 μM concentration.

The collected CD data confirmed the ability of cycTBAs **I-IV** to form a chair-like antiparallel G-quadruplex structure, clearly demonstrating that the cyclization did not impair the G4 structuring ability of TBA nor affected its folding topology, as also previously evidenced in the case of cycTBA.[42]

.

3.2.3. CD thermal denaturation/renaturation measurements

Differences in the behaviour of the cyclic TBA analogues are clearly evident by comparing their CD melting profiles, obtained monitoring the CD signal at 295 nm on varying the temperature. For these experiments, cycTBAs **I-IV** were analysed at 2 μM concentration in both K^+- and Na^+-rich buffer solutions in the 20 - 90 °C range, in comparison with unmodified TBA. In Figure 3 the overlapped CD-melting profiles of cycTBAs **I-IV** are reported in terms of folded fraction as a function of the temperature, while in Figures S13-S16 the overlapped CD-melting and CD-annealing profiles for each compound are shown.

In the K^+-rich buffer (Figure 3a), all the cyclic TBA analogues - except cycTBA **IV** - revealed a noteworthy increased thermal stability compared to unmodified TBA, although exhibiting different behaviours. Indeed, cycTBAs **I**, **II** and **III** (Figures 3a and S13-15a) showed apparent T_m values respectively of ca. 63, 68 and 61 °C (with ΔT_m of + 12, + 17 and + 10 compared to unmodified TBA, Table 2), indicating the formation of very stable G4 structures. Conversely, cycTBA **IV** (Figures 3a and S16a) showed a similar thermal stability as unmodified TBA, with the same apparent T_m values within the experimental error (Table 2).

In the Na^+-rich buffer (Figure 3b) a similar trend was found, with cycTBAs **I** and **II** forming the most stable G4 structures. Notably, the apparent T_m values for these aptamers were respectively of

52 and 59 °C, with a ΔT_m of + 10 and 17 °C vs. unmodified TBA (Table 2, Figures 3b, S13b and S14b). However, in these saline conditions mimicking the extracellular environment, cycTBAs **III** and **IV** (Figures 3b, S15b and S16b) exhibited negligible differences compared to unmodified TBA, showing very similar T_m values (Table 2).

In all cases, a nice sigmoidal behaviour was found (Figures 3 and S13-S16), with no significant hysteresis comparing the heating and cooling profiles, thereby indicating that, under the experimental conditions used (heating rate of 1 °C/min), the related denaturation/renaturation processes were reversible (Figures S13-S16). CD spectra, acquired every 5 °C during each melting and cooling experiment (Figures S17-S20), showed a marked reduction of the CD signals at high temperatures, overall indicating that all the cyclic TBAs behaved as unmodified TBA in both saline phosphate buffers from a qualitative point of view. Notably, all the cyclic analogues were completely denaturated at 90 °C and, after the heating/cooling processes, full recovery of the initial spectral features was always observed (Figures S17-S20).

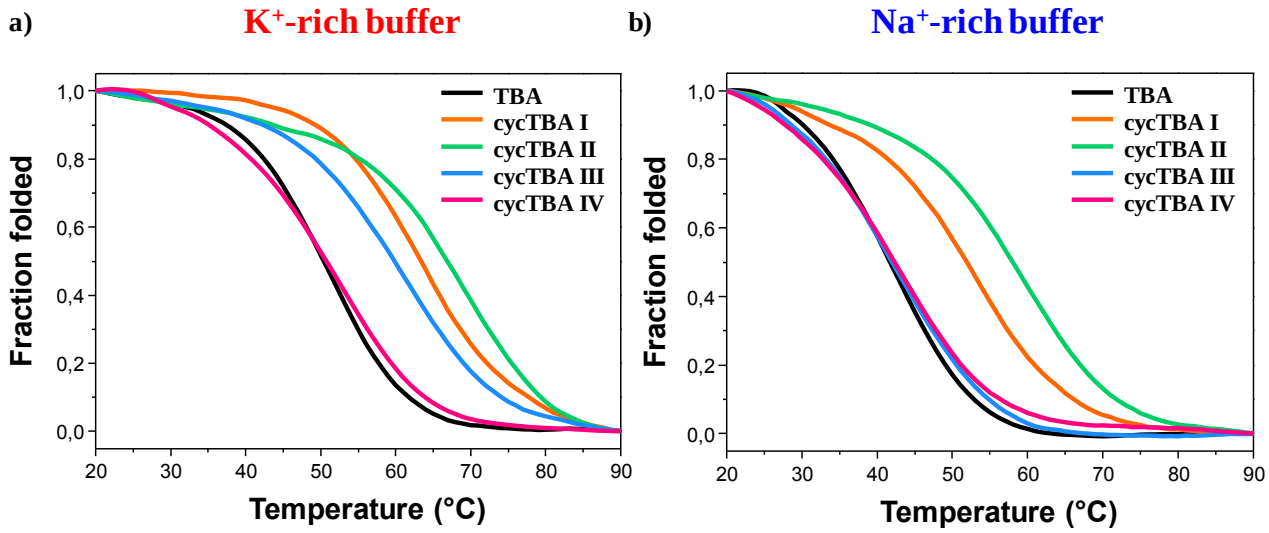

Figure 3. Overlapped CD-melting profiles (recorded at 295 nm, with a heating rate of 1 °C/min) reporting the fraction of folded cycTBAs **I-IV** (orange, green, light blue and magenta lines, respectively) as a function of the temperature, in both the selected K^+- (**a**) and Na^+-rich (**b**) buffers, in comparison to unmodified TBA (black line). All the investigated oligonucleotides were analysed at 2 μM concentration.

The melting curves were also elaborated for van't Hoff analysis, obtaining T_m values consistent with those estimated from the maxima of the first derivative plots. The thermodynamic parameters, the measured apparent T_m as well as the calculated ΔT_m values are shown in Table 2. The enthalpy and entropy change values for unmodified TBA in the K^+-rich solution are in good agreement with those reported in the literature determined under the same conditions.[9,15,64]

https://doi.org/10.1016/j.bioorg.2019.103379

In the case of cycTBAs **I-IV**, all the thermodynamic parameter values are quite similar to those found for unmodified TBA;[9,15,64] and the enthalpy change values are consistent with the destructuring of two G-tetrads.[65–68]

The whole set of thermodynamic analysis data clearly indicated that, compared to unmodified TBA, cycTBA **I** and **II** were the most stable analogues in both buffer solutions; cycTBA **III** exhibited a higher thermal stability in the K^+-rich buffer but not in the Na^+-rich one, while cycTBA **IV** had the same stability as unmodified TBA in both saline conditions. Where observed (i.e. cycTBAs **I-III** in K^+-rich buffer and cycTBAs **I** and **II** in the Na^+-containing solution) the increased energetic stability of these G4 structures is mainly due to a favourable decrease of the unfolding entropy change, in line with the expected structural preorganization of these cyclic aptamers, which balances the slight unfavourable enthalpy decrease.[42]

Taken together, the CD-monitored thermal denaturation data and the related thermodynamic analysis revealed this trend of G4 stability: cycTBA **II** > cycTBA **I** > cycTBA **III** > cycTBA **IV** ≈ TBA in the K^+-rich buffer, and cycTBA **II** > cycTBA **I** > cycTBA **III** ≈ cycTBA **IV** ≈ TBA in the Na^+-rich buffer solution. Particularly, a noteworthy stabilizing effect on the G-quadruplex structure (ΔT_m = + 17) was observed for cycTBA **II** in both saline conditions, behaving very similarly to the previously described cycTBA.[42]

	K^+-rich buffer				
	CD T_m (°C) ± 1	**ΔT_m (°C)**	**$\Delta H_{v.H}$ (kJ mol^{-1})**	**$\Delta S_{v.H}$ (kJ mol^{-1} K^{-1})**	**$\Delta G_{v.H}$ (kJ mol^{-1})**
TBA	51	-	152	0.47	12
cycTBA I	63	+ 12	144	0.43	16
cycTBA II	68	+ 17	141	0.41	19
cycTBA III	61	+ 10	143	0.43	15
cycTBA IV	52	+ 1	130	0.40	11
	Na^+-rich buffer				
	CD T_m (°C) ± 1	**ΔT_m (°C)**	**$\Delta H_{v.H}$ (kJ mol^{-1})**	**$\Delta S_{v.H}$ (kJ mol^{-1} K^{-1})**	**$\Delta G_{v.H}$ (kJ mol^{-1})**
TBA	42	-	147	0.47	7
cycTBA I	52	+ 10	144	0.44	13
cycTBA II	59	+ 17	132	0.40	13
cycTBA III	42	0	127	0.41	8
cycTBA IV	42	0	148	0.47	8

Table 2. Apparent T_m values (estimated from the maxima of the first derivative plots) and thermodynamic parameters ($\Delta H_{v.H}$, $\Delta S_{v.H}$ and $\Delta G_{v.H}$) for the unfolding process of TBA[42] and cycTBAs **I-IV** as determined by CD measurements at 295 nm in both saline phosphate buffer solutions at 2 μM concentration. ΔT_m is calculated by subtracting the measured T_m of unmodified TBA from that observed for each cyclic TBA analogue. $\Delta G_{v.H}$ was calculated at 298 K. Errors on thermodynamic parameters are within ± 10 %, while the error associated with the T_m determination is ± 1 °C.

https://doi.org/10.1016/j.bioorg.2019.103379

3.3. Non-denaturing polyacrylamide gel electrophoresis

In order to further confirm that the cyclic TBA analogues were able to preserve the monomolecular G-quadruplex structure typical of TBA, not forming additional superstructures, a non-denaturing PAGE analysis was carried out. In Figure 4, a representative example of a 15 % polyacrylamide gel - in which cycTBAs **I-IV** were compared with unmodified TBA in both the selected buffer solutions - is reported. Electrophoretic analysis in both saline conditions showed that all the cyclic TBAs migrated as a single band on the gel, with a slightly increased electrophoretic mobility with respect to unmodified TBA.

Taking into account that the gel mobility of the G4 structures is mostly affected by their conformation and compactness and that the charge/mass ratio is very similar for all the here investigated oligonucleotides, PAGE results suggested a more compact structure for all the cyclic aptamers, facilitating their movement through the gel, similarly to what already observed for the previously described cycTBA.[42] This increased mobility is a direct consequence of the cyclic structure of these TBA analogues: in fact, we have previously demonstrated[42] that the migration on the gel of the linear precursor of cycTBA was the same as unmodified TBA, not being affected by the presence of the 3' and 5'-appendages..

Remarkably, no additional retarded bands, attributable to large aggregates or higher order G4 structures, were found, thus indicating the exclusive formation of monomolecular G4 structures, analogously to the case of unmodified TBA.

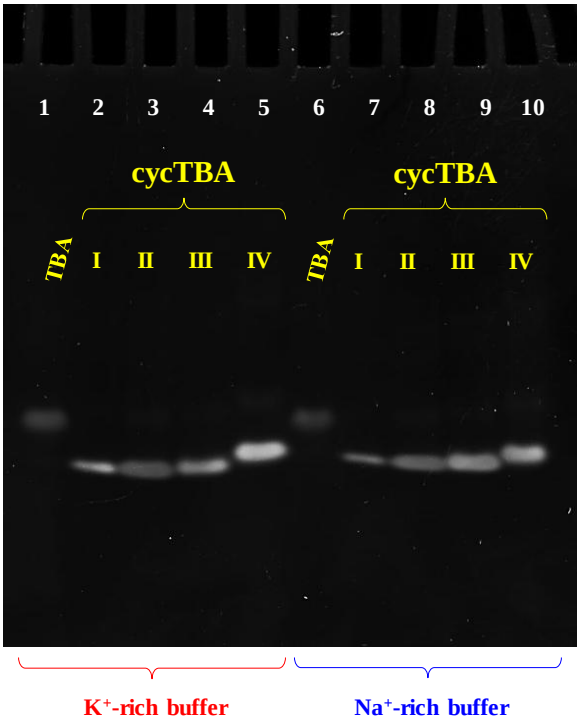

Figure 4. 15 % polyacrylamide gel electrophoresis under native conditions of TBA and the cycTBAs samples at 20 μM concentration in the selected K^+- (lanes 1-5) and Na^+-rich (lanes 6-10) buffer solutions, run at 100 V at r.t. for 75 min in TBE 0.5X buffer; lane 1: TBA; lane 2: cycTBA **I**; lane 3: cycTBA **II**; lane 4: cycTBA **III**; lane 5: cycTBA **IV**; lane 6: TBA; lane 7: cycTBA **I**; lane 8: cycTBA **II** ; lane 9: cycTBA **III**; lane 10: cycTBA **IV**.

3.4. Size exclusion chromatography analysis

Oligonucleotides can adopt a variety of structures depending on the experimental conditions, and the knowledge of their functional conformations in solution is critical to gain insight into their biological role and mechanism. In this context, SE-HPLC recently emerged as a powerful technique to detect the polymorphism of G4 species displaying various structures and/or molecularity and definitively assess the prevailing secondary structures formed by oligonucleotides.[69–71] Thus, its use can be particularly useful to study the conformational behaviour and decipher the polymorphism of G-quadruplexes, in parallel with electrophoretic methods.[72,73]

The analysis of cycTBAs **I-IV** at 2 μM concentration by SE-HPLC analysis showed in all cases only one peak, with retention times of ca. 9 min in both buffer solutions (Figure S21), similar to those found for unmodified TBA, as well as for the previously described cycTBA.[42] These data further supported the native PAGE results, confirming the formation of a unique G4 conformation, comparable to that of unmodified TBA.

Only for cycTBAs **III** and **IV**, a small shoulder under the main peak was detected in both saline conditions, suggesting the possible presence of very low amounts of unstructured cycTBAs or G4 structures with different conformations under the tested conditions. This could be attributed to the presence of long and flexible connecting linkers, which however did not affect the overall conformation and thermal stability of these aptamers, showing in all cases a behaviour very similar to unmodified TBA, as revealed by spectroscopic investigations.

3.5. Nucleases stability assay

The cyclization approach, linking the 5′- and 3′-extremities of the TBA sequence and thus preventing exonuclease attacks, is expected to markedly improve the nuclease resistance of the oligonucleotide, as already demonstrated for the previously reported cycTBA.[42] Thus, cycTBAs **I-IV** were tested in their resistance to nuclease degradation in a pseudo-physiological environment, in order to evaluate the protective effects of cyclization against enzymatic digestion, an event which is typically limiting *in vivo* applications.

cycTBAs **I-IV** - previously annealed and dissolved in PBS - were treated with fetal bovine serum (FBS), using a solution mimicking the extracellular environment in which the aptamer should exert its activity. Thus, in parallel experiments, cycTBAs **I-IV** were incubated in 80 % FBS (v/v) at 37 °C; at fixed times, aliquots of these mixtures were collected and analysed by HPLC on a Nucleogen

https://doi.org/10.1016/j.bioorg.2019.103379

SAX column until disappearance of the peak corresponding to the intact oligonucleotide. The cycTBAs area under their corresponding peak, at each collected time, was then calculated and normalized with respect to the initial one. Percentages of the remaining area of cycTBAs **I**-**IV** are reported in Figure 5, in comparison with unmodified TBA data. Then, fitting of the experimental points allowed the half-life values of the aptamers ($t_{1/2}$). Fitting curves are represented in Figure 5 for an overall view of the nuclease digestion results, but also separately reported for each system in Figure S22.

Overall results clearly indicated that all the cyclic TBAs here investigated had enhanced half-lives with respect to unmodified TBA, used as control (Figure S22).[42] The nuclease stability was found to be not dependent on the specific nature of the linker inserted: in fact, all the derivatives exhibited similar properties, with a closer behaviour between cycTBA **I** and **II**, on one side, and between cycTBA **III** and **IV**, on the other.

In particular, cycTBA **III** and **IV** showed a $t_{1/2}$ of 2.6 h, *i.e.* 4.9-fold higher than unmodified TBA, which under our experimental assay had a half-life of 0.53 h.[42]

The serum nuclease stability of cycTBA **II** was found to be enhanced over TBA by a factor of ca. 6.6 ($t_{1/2}$ = 3.6 h) while cycTBA **I** proved to be the most stable derivative, showing a $t_{1/2}$ of 4.3 h, *i.e.* ca. 8.1-fold higher than TBA. The general trend of serum nuclease resistance was therefore: cycTBA **I** > cycTBA **II** > cycTBA **III** ≈ cycTBA **IV** >> TBA.

These data comprehensively supported the initial idea that end-capped G4 structures - as those obtained by cyclization of the 5′ and 3′-ends - are indeed less accessible to the nuclease attack than the G4 structure formed by unmodified TBA.

https://doi.org/10.1016/j.bioorg.2019.103379

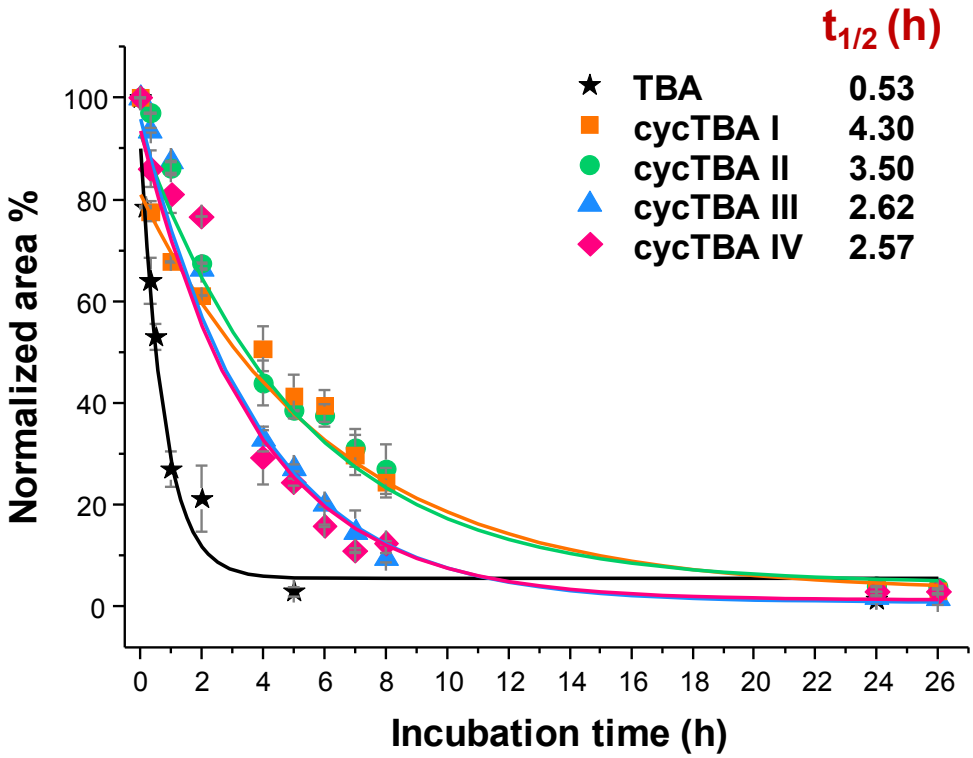

Figure 5. Enzymatic resistance experiments on TBA and cycTBAs **I-IV** incubated in 80 % fetal bovine serum (FBS) as monitored by SAX-HPLC analysis up to 26 h. Chromatographic peak area is expressed as percentage of the each cyclic TBA remaining area (see legend for detail) normalized to the initial one for all the analysed time points (8 and 11 total time points collected in 1 day, respectively for TBA and cycTBAs **I-IV**). Data are reported as mean values ± SD (error bars) for multiple determinations. Obtained values were also fitted with an equation for first order kinetics, allowing the determination of the half-life of each aptamer ($t_{1/2}$).

3.6. Coagulation experiments

The ability of cycTBAs **I-IV** to inhibit the thrombin-catalysed conversion of fibrinogen into fibrin was investigated by means of light scattering experiments and compared with that of unmodified TBA. The analysis of the normalized autocorrelation functions gives a direct information on the size of the species in the system, so we analysed the autocorrelation functions obtained for the different systems upon 5 min monitoring from the beginning of the experiment (Figure S23). The two limit cases are represented by the autocorrelation functions of the sample only containing fibrinogen - which had a well-defined sigmoidal shape and whose position did not change with time - and that of the sample containing fibrinogen and thrombin but no anticoagulant agent, which, already after 5 min, was sensibly shifted towards long delay times and did not reach zero even at very long times, clearly indicating the formation of very big, barely soluble aggregates. Samples containing anticoagulant aptamers, either cycTBAs **I-IV** or native TBA, showed an intermediate behaviour between these two limit cases. In particular, the autocorrelation function of the sample containing cycTBA **I** was close to that of the sample only containing thrombin, but in the long run

reached zero, indicating the presence in solution of still soluble, smaller species. The curves of the TBA-, cycTBA **III**- or cycTBA **IV**-containing samples were very close to each other, suggesting the presence of even smaller species than those present in the case of cycTBA **I**. Finally, the autocorrelation curve found for the cycTBA **II**-containing sample was the closest to the fibrinogen autocorrelation curve, indicating a sensibly retarded coagulation process.

Overall, the analysis of the autocorrelation functions clearly proved that the TBA cyclization overall affected the thrombin recognition/inhibition properties of the here tested aptamers and, at the same time, highlighted different inhibiting ability of cycTBAs **I-IV**. Same results were obtained when the scattered intensity was monitored (Figure 6a). Indeed, a rapid increase of the scattered intensity with time, indicating the progression of fibrin formation, was found in the samples only containing fibrinogen and thrombin, while when cycTBAs **I-IV** or unmodified TBA were added, the scattered intensity increased much more slowly than in the untreated samples, evidencing the net inhibition of thrombin coagulation activity (Figure 6a). The extent of the scattered intensity increase depended on the used aptamer, indicating again that cycTBAs **I-IV** displayed different anticoagulant properties. Thus, to quantitatively assess the anti-thrombin activity of cycTBAs **I-IV** and to compare it with that of unmodified TBA, we calculated the anticoagulant efficacy of each aptamer as the ratio between the coagulation rates, defined as the slope of the line fitting the initial increase of the normalized scattering intensity plotted as a function of time, in the exclusive presence of thrombin and in the presence of both thrombin and each tested aptamer. The results, reported in Figure 6b, notably showed cycTBA **II** as a more effective anticoagulant agent than TBA, while cycTBA **III** and cycTBA **IV** behaved similarly to the first developed cycTBA[42] proving to be slightly less potent than TBA. Interestingly, cycTBA **I** was the less potent aptamer of the investigated series.

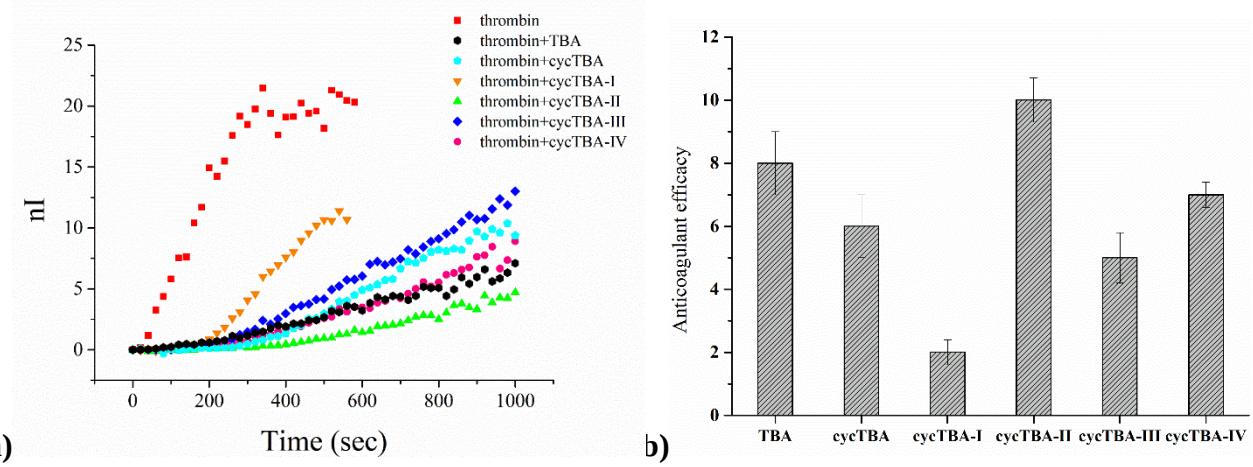

Figure 6. a) Coagulation curves of fibrinogen in the presence of thrombin and different anticoagulant agents (TBA; cycTBA; cycTBAs **I-IV**, see inset for details) at thrombin:aptamer 1:5 molar ratio.

https://doi.org/10.1016/j.bioorg.2019.103379

b) Coagulation efficacy (defined as the ratio between the coagulation rate in the exclusive presence of thrombin and in the presence of both thrombin and each aptamer) of cycTBAs **I-IV** with respect to unmodified TBA and cycTBA.

4. CONCLUSIONS

Among the known aptamers able to fold into stable G-quadruplex structures, TBA is probably the most studied system, object of wide investigations for its intriguing therapeutic and diagnostic potential, and also used as effective tool to validate sensing strategies.[6]

In a recent communication,[42] we anticipated that the TBA properties could be markedly improved by covalently linking the extremities of its sequence. Indeed, as a proof-of-concept we prepared a first TBA analogue circularized via a 20 atom-long linker, which exhibited a remarkable serum resistance and a notably increased thermal stability of its G-quadruplex core. Unfortunately, its binding affinity to thrombin and anticoagulant activity were sensibly reduced compared to native TBA.[42]

Thus, stimulated by the favourable impact of cyclization on the aptamer biophysical properties, in the present work we prepared a small library of novel cyclic TBA derivatives containing different flexible circularizing linkers of variable length, ranging from 22 to 48 atoms. Our aim was to obtain a good compromise between increasing the compactness of the aptamer G-quadruplex core, necessary to improve the oligonucleotide resistance to nucleases, and maintaining some structural flexibility, somehow crucial for thrombin recognition.

Four novel derivatives were thus prepared: in particular, cycTBAs **I** and **II** were circularized by using the oxime ligation method, while cycTBAs **III** and **IV** were obtained using a Cu(I)-catalysed azide-alkyne cycloaddition approach. With this series of novel cyclic TBAs, we have therefore tested and compared two different cyclization procedures, both providing in high yields and few synthetic steps the desired cyclic aptamers, characterized by connecting linkers with different chemical properties and peculiar structural elements.

Then, we investigated the structural and biophysical properties of these cyclic TBA analogues by using a combined approach including spectroscopic, electrophoretic as well as chromatographic techniques. UV and CD spectroscopic data confirmed that cycTBAs **I-IV** adopted antiparallel, chair-like G-quadruplex conformations, essentially similar to that of their natural counterpart. The thermal stability of these structures was strictly solution-dependent. In fact, the melting temperatures of cycTBAs **I-IV** were in all cases higher than that of unmodified TBA (ΔT_m ranging from +1 to +17 °C) in a K^+-rich buffer solution, while, in the case of a Na^+-rich medium, only cycTBAs **I** and **II** proved to be more stable than unmodified TBA, with ΔT_m of +10 and +17 °C, respectively. In all the studied buffer solutions, cycTBA **II** showed the most favourable

thermodynamic properties, indicating that its 30 atom-long circularizing linker ensured the highest stabilization of the G4 structure in the investigated series.

Most importantly, the serum resistance of cycTBAs **I-IV** proved to be always increased with respect to TBA. Indeed, cycTBAs **I** and **II** showed a 8.1- and 6.6-fold enhancement in stability to nuclease digestion, with $t_{1/2}$ of 4.3 and 3.5 h, respectively, while cycTBAs **III** and **IV** displayed a 4.9-fold increased stability, with $t_{1/2}$ values slightly lower than 3 h.

Finally, light scattering experiments showed cycTBA **II** as the most potent anticoagulant agent, with a higher thrombin clotting inhibitory activity than unmodified TBA and the other cycTBAs.

Thus, the obtained results demonstrated an effective dependence of the chemical properties and anticoagulant activity of the synthesized cyclic analogues of TBA on varying the length and nature of the circularizing linker. In particular, among all the designed derivatives, the best candidate proved to be cycTBA **II**. In this compound the linker of 30 atoms length seems to nicely combine, on one hand, a marked stabilization of the G-quadruplex core and an increased nuclease resistance, and, on the other hand, an improved anticoagulant activity with respect to both unmodified TBA and the previously developed cyclic analogue. Interestingly, the lipophilic benzene ring in the connecting linker could also play a role in the observed enhanced stability by establishing additional stacking interactions with the G-tetrads, finally promoting the G4 structuring and subsequent recognition/inhibition of the protein.

In contrast, in the case of cycTBA **I**, carrying a linker very similar in length to our first prototype cycTBA but containing one additional nucleotide, and thus one additional phosphate unit, the higher stability of the G4 core and the enhanced resistance to nuclease digestion was not accompanied by an improved thrombin inhibition activity, in contrast proving to be the worst inhibitor of the series. The case of cycTBA **I** indicates that, as also observed for cycTBA,[42] a short linker (20-22 atoms) also including additional rigid structural elements somehow prevented the optimal recognition/interaction with the protein.

In turn, cycTBAs **III** and **IV** showed a similar behaviour, with little or no stabilization of the G-quadruplex structure, a higher but not exceptional resistance to enzymatic degradation and a reduced antithrombin activity compared to unmodified TBA. In these cyclic analogues, the linker is probably too long (34-48 atoms), somehow causing steric hindrance and/or too much flexibility to the system. As in the case of cycTBA **I**, the presence of additional phosphates (respectively one and two for cycTBAs **III** and **IV**) could also play a role, impairing G-quadruplex structuring and target recognition.

Taken together, the present data also demonstrated that the anticoagulant efficacy of TBA analogues is controlled by multiple phenomena, in which the aptamer enzymatic stability and structural preorganization of their functional folding are only one side of the coin.

Indeed, our results confirmed that a very high rigidity may be detrimental for an effective thrombin binding and inhibition, as suggested in our previous work,[42] highlighting that long and bulky modifications can also hamper the thrombin-aptamer interaction due to steric hindrance. Finally, the interaction with the target protein seems to be negatively affected by the insertion of additional phosphate groups in the linker, that likely alter the delicate balance between electrostatic and apolar interactions leading to effective thrombin-aptamer recognition.

The remarkable thermal stability and the general properties of cycTBA **II**, incorporating a flexible circularizing 30 atom-long linker without additional phosphate groups, suggest that this modification could be successfully extended also to other G-quadruplex-forming aptamers to enhance their properties so to develop new, efficient tools for biomedical, supramolecular chemistry and nanotechnology applications.[4]

Acknowledgements

This work was supported by the Italian Association for Cancer Research (AIRC) (IG2015 n. 17037 to D.M.). F. M. is member of INSERM.

REFERENCES:

[1] A. Aviñó, C. Fàbrega, M. Tintoré, R. Eritja, Thrombin binding aptamer, more than a simple aptamer: chemically modified derivatives and biomedical applications., Curr. Pharm. Des. 18 (2012) 2036–47. doi:10.1128/AAC.03728-14.

[2] D. Musumeci, D. Montesarchio, Polyvalent nucleic acid aptamers and modulation of their activity: a focus on the thrombin binding aptamer, Pharmacol. Ther. 136 (2012) 202–215. doi:10.1016/j.pharmthera.2012.07.011.

[3] E. Zavyalova, N. Ustinov, A. Golovin, G. Pavlova, A. Kopylov, G-quadruplex aptamers to human thrombin versus other direct thrombin inhibitors: the focus on mechanism of action and drug efficiency as anticoagulants., Curr. Med. Chem. 23 (2016) 2230–2244. doi:10.2174/0929867323666616031612508.

[4] C. Platella, C. Riccardi, D. Montesarchio, G.N. Roviello, D. Musumeci, G-quadruplex-based aptamers against protein targets in therapy and diagnostics, BBA - Gen. Subj. 1861 (2017) 1429–1447. doi:10.1016/j.bbagen.2016.11.027.

[5] A. Schwienhorst, Direct thrombin inhibitors - a survey of recent developments, Cell. Mol.

Life Sci. 63 (2006) 2773–2791. doi:10.1007/s00018-006-6219-z.

[6] D. Musumeci, C. Platella, C. Riccardi, F. Moccia, D. Montesarchio, Fluorescence sensing using DNA aptamers in cancer research and clinical diagnostics, Cancers. 9 (2017) 174–217. doi:10.3390/cancers9120174.

[7] I. Smirnov, R.H. Shafer, Effect of Loop Sequence and Size on DNA Aptamer Stability, Biochemistry. 39 (2000) 1462–1468.

[8] B. Sacca, L. Lacroix, J.-L. Mergny, The effect of chemical modifications on the thermal stability of different G-quadruplex-forming oligonucleotides, Nucleic Acids Res. 33 (2005) 1182–1192. doi:10.1093/nar/gki257.

[9] L. Martino, A. Virno, A. Randazzo, A. Virgilio, V. Esposito, C. Giancola, M. Bucci, G. Cirino, L. Mayol, A new modified thrombin binding aptamer containing a 5′-5′ inversion of polarity site, Nucleic Acids Res. 34 (2006) 6653–6662. doi:10.1093/nar/gkl915.

[10] C.G. Peng, M.J. Damha, G-quadruplex induced stabilization by 2′-deoxy-2′-fluoro-d-arabinonucleic acids (2′F-ANA), Nucleic Acids Res. 35 (2007) 4977–4988. doi:10.1093/nar/gkm520.

[11] S. Nagatoishi, N. Isono, K. Tsumoto, N. Sugimoto, Loop residues of thrombin-binding DNA aptamer impact G-quadruplex stability and thrombin binding, Biochimie. 93 (2011) 1231–1238. doi:10.1016/j.biochi.2011.03.013.

[12] A. Pasternak, F.J. Hernandez, L.M. Rasmussen, B. Vester, J. Wengel, Improved thrombin binding aptamer by incorporation of a single unlocked nucleic acid monomer, Nucleic Acids Res. 39 (2011) 1155–1164. doi:10.1093/nar/gkq823.

[13] N. Borbone, M. Bucci, G. Oliviero, E. Morelli, J. Amato, V. D'Atri, S.D. D'Errico, V. Vellecco, G. Cirino, G. Piccialli, C. Fattorusso, M. Varra, L. Mayol, M. Persico, M. Scuotto, Investigating the role of T7 and T12 residues on the biological properties of thrombin-binding aptamer: enhancement of anticoagulant activity by a single nucleobase modification, J. Med. Chem. 55 (2012) 10716–10728. doi:10.1021/jm301414f.

[14] S. De Tito, F. Morvan, A. Meyer, J.J. Vasseur, A. Cummaro, L. Petraccone, B. Pagano, E. Novellino, A. Randazzo, C. Giancola, D. Montesarchio, Fluorescence enhancement upon G-quadruplex folding: synthesis, structure, and biophysical characterization of a dansyl/cyclodextrin-tagged thrombin binding aptamer, Bioconjugate Chem. 24 (2013) 1917–1927. doi:10.1021/bc400352s.

[15] A. Virgilio, L. Petraccone, V. Vellecco, M. Bucci, M. Varra, C. Irace, R. Santamaria, A. Pepe, L. Mayol, V. Esposito, A. Galeone, Site-specific replacement of the thymine methyl group by fluorine in thrombin binding aptamer significantly improves structural stability and

anticoagulant activity, Nucleic Acids Res. 43 (2015) 10602–10611. doi:10.1093/nar/gkv1224.

[16] M. Scuotto, E. Rivieccio, A. Varone, D. Corda, M. Bucci, V. Vellecco, G. Cirino, A. Virgilio, V. Esposito, A. Galeone, N. Borbone, M. Varra, L. Mayol, Site specific replacements of a single loop nucleoside with a dibenzyl linker may switch the activity of TBA from anticoagulant to antiproliferative, Nucleic Acids Res. 43 (2015) 7702–7716. doi:10.1093/nar/gkv789.

[17] V. Esposito, A. Russo, T. Amato, M. Varra, V. Vellecco, M. Bucci, G. Russo, A. Virgilio, A. Galeone, Backbone modified TBA analogues endowed with antiproliferative activity, Biochim. Biophys. Acta - Gen. Subj. 1861 (2017) 1213–1221. doi:10.1016/j.bbagen.2016.09.019.

[18] W. Kotkowiak, J. Lisowiec-Wachnicka, J. Grynda, R. Kierzek, J. Wengel, A. Pasternak, Thermodynamic, anticoagulant, and antiproliferative properties of thrombin binding aptamer containing novel UNA derivative, Mol. Ther. - Nucleic Acids. 10 (2018) 304–316. doi:10.1016/j.omtn.2017.12.013.

[19] Z. Chai, L. Guo, H. Jin, Y. Li, S. Du, Y. Shi, C. Wang, W. Shi, J. He, TBA loop mapping with 3′-inverted-deoxythymidine for fine-tuning of the binding affinity for α-thrombin, Org. Biomol. Chem. 17 (2019) 2403–2412. doi:10.1039/c9ob00053d.

[20] M.V. Yigit, D. Mazumdar, Y. Lu, MRI detection of thrombin with aptamer functionalized superparamagnetic iron oxide nanoparticles, Bioconjugate Chem. 19 (2008) 412–417. doi:10.1021/bc7003928.

[21] D. Musumeci, G. Oliviero, G.N. Roviello, E.M. Bucci, G. Piccialli, G-quadruplex-forming oligonucleotide conjugated to magnetic nanoparticles: synthesis, characterization, and enzymatic stability assays, Bioconjugate Chem. 23 (2012) 382–391. doi:10.1021/bc200305t.

[22] J.M. Yu, L.R. Yang, X.F. Liang, T.T. Dong, H.Z. Liu, Bare magnetic nanoparticles as fluorescence quenchers for detection of thrombin, Analyst. 140 (2015) 4114–4120. doi:10.1039/c5an00519a.

[23] Y.C. Shiang, C.C. Huang, T.H. Wang, C.W. Chien, H.T. Chang, Aptamer-conjugated nanoparticles efficiently control the activity of thrombin, Adv. Funct. Mater. 20 (2010) 3175–3182. doi:10.1002/adfm.201000642.

[24] Y.C. Shiang, C.L. Hsu, C.C. Huang, H.T. Chang, Gold nanoparticles presenting hybridized self-assembled aptamers that exhibit enhanced inhibition of thrombin, Angew. Chem. - Int. Ed. Eng. 50 (2011) 7660–7665. doi:10.1002/anie.201101718.

[25] C.L. Hsu, H.T. Chang, C.T. Chen, S.C. Wei, Y.C. Shiang, C.C. Huang, Highly efficient

control of thrombin activity by multivalent nanoparticles, Chem. Eur. J. 17 (2011) 10994–11000. doi:10.1002/chem.201101081.

[26] C.L. Hsu, S.C. Wei, J.W. Jian, H.T. Chang, W.H. Chen, C.C. Huang, Highly flexible and stable aptamer-caged nanoparticles for control of thrombin activity, RSC Adv. 2 (2012) 1577–1584. doi:10.1039/c1ra00344e.

[27] S.S. Huang, S.C. Wei, H.T. Chang, H.J. Lin, C.C. Huang, Gold nanoparticles modified with self-assembled hybrid monolayer of triblock aptamers as a photoreversible anticoagulant, J. Control. Release. 221 (2016) 9–17. doi:10.1016/j.jconrel.2015.11.028.

[28] L. Gao, Y. Cui, Q. He, Y. Yang, J. Fei, J. Li, Selective recognition of co-assembled thrombin aptamer and docetaxel on mesoporous silica nanoparticles against tumor cell proliferation, Chem. Eur. J. 17 (2011) 13170–13174. doi:10.1002/chem.201101658.

[29] E. Babu, P.M. Mareeswaran, S. Rajagopal, Highly sensitive optical biosensor for thrombin based on structure switching aptamer-luminescent silica nanoparticles, J. Fluoresc. 23 (2013) 137–146. doi:10.1007/s10895-012-1127-0.

[30] Q. Yue, T. Shen, L. Wang, S. Xu, H. Li, Q. Xue, Y. Zhang, X. Gu, S. Zhang, J. Liu, A convenient sandwich assay of thrombin in biological media using nanoparticle-enhanced fluorescence polarization, Biosens. Bioelectron. 56 (2014) 231–236. doi:10.1016/j.bios.2014.01.021.

[31] C. Riccardi, I. Russo Krauss, D. Musumeci, F. Morvan, A. Meyer, J.J. Vasseur, L. Paduano, D. Montesarchio, Fluorescent thrombin binding aptamer-tagged nanoparticles for an efficient and reversible control of thrombin activity, ACS Appl. Mater. Interfaces. 9 (2017) 35574–35587. doi:10.1021/acsami.7b11195.

[32] P.X. Lai, J.Y. Mao, B. Unnikrishnan, H.W. Chu, C.W. Wu, H.T. Chang, C.C. Huang, Self-assembled, bivalent aptamers on graphene oxide as an efficient anticoagulant, Biomater. Sci. 6 (2018) 1882–1891. doi:10.1039/c8bm00288f.

[33] T.-X. Lin, P.-X. Lai, J.-Y. Mao, H.-W. Chu, B. Unnikrishnan, A. Anand, C.-C. Huang, Supramolecular Aptamers on Graphene Oxide for Efficient Inhibition of Thrombin Activity, Front. Chem. 7 (2019). doi:0.3389/fchem.2019.00280.

[34] N. Riahifard, S. Mozaffari, T. Aldakhil, F. Nunez, Q. Alshammari, J. Yamaki, K. Parang, R.K. Tiwari, Design, synthesis, and evaluation of amphiphilic cyclic and linear peptides composed of hydrophobic and positively-charged amino acids as antibacterial agents., Molecules. 23 (2018) 2722. doi:10.3390/molecules23102722.

[35] N. Qvit, S.J.S. Rubin, T.J. Urban, D. Mochly-Rosen, E.R. Gross, Peptidomimetic therapeutics: scientific approaches and opportunities, Drug Discov. Today. 22 (2017) 454–

462. doi:10.1016/j.drudis.2016.11.003.

[36] L. Moggio, L. De Napoli, B. Di Blasio, G. Di Fabio, J. D'Onofrio, D. Montesarchio, A. Messere, Solid-phase synthesis of cyclic PNA and PNA-DNA chimeras, Org. Lett. 8 (2006) 2015–2018. doi:10.1021/ol0603559.

[37] G. Di Fabio, A. Randazzo, J. D'Onofrio, C. Ausín, E. Pedroso, A. Grandas, L. De Napoli, D. Montesarchio, Cyclic phosphate-linked oligosaccharides: synthesis and conformational behavior of novel cyclic oligosaccharide analogues, J. Org. Chem. 71 (2006) 3395–3408. doi:10.1021/jo0600757.

[38] C. Coppola, V. Saggiomo, G. Di Fabio, L. De Napoli, D. Montesarchio, Novel amphiphilic cyclic oligosaccharides: synthesis and self-aggregation properties, J. Org. Chem. 72 (2007) 9679–9689. doi:10.1021/jo7017087.

[39] L. De Napoli, A. Messere, D. Montesarchio, G. Piccialli, C. Santacroce, G.M. Bonora, PEG-supported synthesis of cyclic oligodeoxyribonucleotides, Nucleosides and Nucleotides. 12 (1993) 21–30. doi:10.1080/07328319308016191.

[40] J. Lietard, A. Meyer, J.J. Vasseur, F. Morvan, New strategies for cyclization and bicyclization of oligonucleotides by click chemistry assisted by microwaves, J. Org. Chem. 73 (2008) 191–200. doi:10.1021/jo702177c.

[41] D.A. Di Giusto, G.C. King, Construction, stability, and activity of multivalent circular anticoagulant aptamers, J. Biol. Chem. 279 (2004) 46483–46489. doi:10.1074/jbc.M408037200.

[42] C. Riccardi, A. Meyer, J.J. Vasseur, I. Russo Krauss, L. Paduano, R. Oliva, L. Petraccone, F. Morvan, D. Montesarchio, Stability is not everything: the case of the cyclization of the thrombin binding aptamer, ChemBioChem. 20 (2019) 1789–1794. doi:10.1002/cbic.201900045.

[43] I. Russo Krauss, A. Merlino, C. Giancola, A. Randazzo, L. Mazzarella, F. Sica, Thrombin-aptamer recognition: a revealed ambiguity, Nucleic Acids Res. 39 (2011) 7858–7867. doi:10.1093/nar/gkr522.

[44] I. Russo Krauss, A. Merlino, A. Randazzo, E. Novellino, L. Mazzarella, F. Sica, High-resolution structures of two complexes between thrombin and thrombin-binding aptamer shed light on the role of cations in the aptamer inhibitory activity, Nucleic Acids Res. 40 (2012) 8119–8128. doi:10.1093/nar/gks512.

[45] R. Troisi, V. Napolitano, V. Spiridonova, I. Russo Krauss, F. Sica, Several structural motifs cooperate in determining the highly effective anti-thrombin activity of NU172 aptamer, Nucleic Acids Res. 46 (2018) 12177–12185. doi:10.1093/nar/gky990.

[46] O.P. Edupuganti, E. Defrancq, P. Dumy, Head-to-Tail oxime cyclization of oligodeoxynucleotides for the efficient synthesis of circular DNA analogues, J. Org. Chem. 68 (2003) 8708–8710. doi:10.1021/jo035064h.

[47] A. Meyer, J.J. Vasseur, P. Dumy, F. Morvan, Phthalimide–oxy derivatives for 3′- or 5′-conjugation of oligonucleotides byoOxime ligation and circularization of DNA by "bis- or tris-Click" oxime ligation, Eur. J. Org. Chem. (2017) 6931–6941. doi:10.1002/ejoc.201701317.

[48] G. Pourceau, A. Meyer, J.J. Vasseur, F. Morvan, Azide solid support for 3′-conjugation of oligonucleotides and their circularization by click chemistry, J. Org. Chem. 74 (2009) 6837–6842. doi:10.1021/jo9014563.

[49] F. Morvan, (2019), *submitted manuscript*.

[50] J.-L. Mergny, J. Li, L. Lacroix, S. Amrane, J.B. Chaires, Thermal difference spectra: a specific signature for nucleic acid structures, Nucleic Acids Res. 33 (2005) 1–6. doi:10.1093/nar/gni134.

[51] J.-L. Mergny, L. Lacroix, UV Melting of G-Quadruplexes, Curr. Protoc. Nucleic Acid Chem. 37 (2009) 17.1.1-17.1.15. doi:10.1002/0471142700.nc1701s37.

[52] M. Malgowska, D. Gudanis, A. Teubert, G. Dominiak, Z. Gdaniec, How to study G-quadruplex structures, J. Biotechnol. Comput. Biol. Bionanotechnol. 93 (2012) 381–390. doi:10.5114/bta.2012.46592.

[53] L.A. Marky, K.J. Breslauer, Calculating thermodynamic data for transitions of any molecularity from equilibrium melting curves, Biopolymers. 26 (1987) 1601–1620. doi:10.1002/bip.360260911.

[54] C.C. Hardin, T. Watson, M. Corregan, C. Bailey, Cation-dependent transition between the quadruplex and Watson-Crick hairpin forms of d(CGCG$_3$GCG), Biochemistry. 31 (1992) 833–841. doi:10.1021/bi00118a028.

[55] N. V Hud, F.W. Smith, F.A.L. Anet, J. Feigon, The selectivity for K^+ versus Na^+ in DNA quadruplexes is dominated by relative free energies of hydration: a thermodynamic analysis by ^{1}H NMR, Biochemistry. 35 (1996) 15383–15390. doi:10.1021/bi9620565.

[56] S. Poniková, M. Antalík, T. Hianik, A circular dichroism study of the stability of guanine quadruplexes of thrombin DNA aptamers at presence of K^+ and Na^+ ions, Gen. Physiol. Biophys. 27 (2008) 271–277.

[57] E. Zavyalova, G. Tagiltsev, R. Reshetnikov, A. Arutyunyan, A. Kopylov, Cation coordination alters the conformation of a thrombin-binding G-quadruplex DNA aptamer that affects inhibition of thrombin, Nucleic Acid Ther. 6 (2016) 299–308.

doi:10.1089/nat.2016.0606.

[58] V. Dapić, V. Abdomerović, R. Marrington, J. Peberdy, A. Rodger, J.O. Trent, P.J. Bates, Biophysical and biological properties of quadruplex oligodeoxyribonucleotides, Nucleic Acids Res. 31 (2003) 2097–2107. doi:10.1093/nar/gkg316.

[59] S. Paramasivan, I. Rujan, P.H. Bolton, Circular dichroism of quadruplex DNAs: applications to structure, cation effects and ligand binding, Methods. 43 (2007) 324–331. doi:10.1016/j.ymeth.2007.02.009.

[60] J. Kypr, I. Kejnovská, D. Renčiuk, M. Vorlíčková, Circular dichroism and conformational polymorphism of DNA, Nucleic Acids Res. 37 (2009) 1713–1725. doi:10.1093/nar/gkp026.

[61] S. Masiero, R. Trotta, S. Pieraccini, S. De Tito, R. Perone, A. Randazzo, G.P. Spada, A non-empirical chromophoric interpretation of CD spectra of DNA G-quadruplex structures, Org. Biomol. Chem. 8 (2010) 2683–2692. doi:10.1039/c003428b.

[62] A.I. Karsisiotis, N.M.A. Hessari, E. Novellino, G.P. Spada, A. Randazzo, M. Webba da Silva, Topological characterization of nucleic acid G-Quadruplexes by UV absorption and circular dichroism, Angew. Chemie - Int. Ed. Eng. 50 (2011) 10645–10648. doi:10.1002/anie.201105193.

[63] M. Vorlíčková, I. Kejnovská, J. Sagi, D. Renčiuk, K. Bednářová, J. Motlová, J. Kypr, Circular dichroism and guanine quadruplexes, Methods. 57 (2012) 64–75. doi:10.1016/j.ymeth.2012.03.011.

[64] A. Virno, A. Randazzo, C. Giancola, M. Bucci, G. Cirino, L. Mayol, A novel thrombin binding aptamer containing a G-LNA residue, Bioorg. Med. Chem. 15 (2007) 5710–5718. doi:10.1016/j.bmc.2007.06.008.

[65] L. Petraccone, E. Erra, L. Nasti, A. Galeone, A. Randazzo, L. Mayol, G. Barone, C. Giancola, Effect of a modified thymine on the structure and stability of $[d(TGGGT)]_4$ quadruplex, Int. J. Biol. Macromol. 31 (2003) 131–137. doi:10.1016/S0141-8130(02)00073-9.

[66] L. Petraccone, E. Erra, V. Esposito, A. Randazzo, L. Mayol, L. Nasti, G. Barone, C. Giancola, Stability and structure of telomeric DNA sequences forming quadruplexes containing four G-tetrads with different topological arrangements, Biochemistry. 43 (2004) 4877–4884. doi:10.1021/bi0300985.

[67] C.M. Olsen, W.H. Gmeiner, L.A. Marky, Unfolding of G-quadruplexes: energetic, and ion and water contributions of G-quartet stacking, J. Phys. Chem. B. 110 (2006) 6962–6969. doi:10.1021/jp0574697.

[68] L. Petraccone, C. Spink, J.O. Trent, N.C. Garbett, C.S. Mekmaysy, C. Giancola, J.B. Chaires,

Structure and stability of higher-order human telomeric quadruplexes, J. Am. Chem. Soc. 133 (2011) 20951–20961. doi:10.1021/ja209192a.

[69] M.M. Dailey, M. Clarke Miller, P.J. Bates, A.N. Lane, J.O. Trent, Resolution and characterization of the structural polymorphism of a single quadruplex-forming sequence, Nucleic Acids Res. 38 (2010) 4877–4888. doi:10.1093/nar/gkq166.

[70] E. Largy, J.-L. Mergny, Shape matters: size-exclusion HPLC for the study of nucleic acid structural polymorphism, Nucleic Acids Res. 42 (2014) e149. doi:10.1093/nar/gku751.

[71] E.G. Zavyalova, V.A. Legatova, R.S. Alieva, A.O. Zalevsky, V.N. Tashlitsky, A.M. Arutyunyan, A.M. Kopylov, Putative mechanisms underlying high inhibitory activities of bimodular DNA aptamers to thrombin, Biomolecules. 9 (2019) 1–15. doi:10.3390/biom9020041.

[72] C. Riccardi, D. Musumeci, I. Russo Krauss, M. Piccolo, C. Irace, L. Paduano, D. Montesarchio, Exploring the conformational behaviour and aggregation properties of lipid-conjugated AS1411 aptamers, Int. J. Biol. Macromol. 118 (2018) 1384–1399. doi:10.1016/j.ijbiomac.2018.06.137.

[73] F. Moccia, C. Riccardi, D. Musumeci, S. Leone, R. Oliva, L. Petraccone, D. Montesarchio, Insights into the G-rich VEGF-binding aptamer V7t1: when two G-quadruplexes are better than one!, Nucleic Acids Res. (2019). doi:10.1093/nar/gkz589.